Earth and Planetary Science Letters 357–358 (2012) 152–167

Contents lists available at SciVerse ScienceDirect

Earth and Planetary Science Letters

journal homepage: www.elsevier.com/locate/epsl

Holocene shortening across the Main Frontal Thrust zone in the eastern Himalaya

W. Paul Burgess [a], An Yin [a,*], Chandra S. Dubey [b], Zheng-Kang Shen [a], Thomas K. Kelty [c]

[a] Department of Earth and Space Sciences and Institute for Planets and Exoplanets (iPLEX), University of California, Los Angeles, CA 90095-1567, United States
[b] Department of Geology, Delhi University, Delhi 110007, India
[c] Department of Geological Sciences, California State University at Long Beach, Long Beach, CA 90840-3902, United States

ARTICLE INFO

Article history:
Received 10 May 2012
Received in revised form
22 September 2012
Accepted 24 September 2012
Editor: P. Shearer
Available online 18 October 2012

Keywords:
Himalayan orogen
Main Frontal Thrust zone
active tectonics
Himalayan tectonics

ABSTRACT

How plate-boundary processes control intra-continental deformation is a fundamental question in Earth sciences. Although it is long known that the active India–Asia convergence rate increases eastward, how this boundary condition impacts on active growth of the Himalaya is unclear. To address this issue, we conducted a geologic investigation of the Main Frontal Thrust (MFT), the largest and the most dominant active structure in the Himalayan orogen. Using the age and geometry of uplifted river terraces, we establish a minimum Holocene slip rate of 23 ± 6.2 mm/yr along the decollement of the 10 km wide MFT zone in the far eastern Himalaya. This slip rate is partitioned on three structures: at $\sim$8.4 mm/yr on the Bhalukpong thrust in the north, at $\sim$10 mm/yr across the growing Balipara anticline in the middle, and at $\sim$5 mm/yr on the Nameri thrust in the south. Our estimated minimum total shortening rate is significantly higher than the Holocene slip rate of 9 ± 3 mm/yr for the MFT in the western Himalaya. However, this rate is similar to or potentially greater than the slip rate of 21 ± 1.5 mm/yr for the MFT in the central Himalaya. Our results support an early interpretation that active shortening across the Himalayan orogen is mostly accommodated by slip along the narrow MFT zone and its linked decollement beneath the Himalaya. The eastward increase in the Holocene MFT slip rate requires that the plate-boundary force rather than gravitational spreading is the fundamental control on active growth of the Himalayan orogen.

1. Introduction

The 2500 km Himalayan Main Frontal Thrust (MFT) zone is the longest active contractional structure in the largest active collisional orogen on Earth (e.g., Gansser, 1964; Nakata, 1989; Yeats et al., 1992; Bilham et al., 1998; Lavé and Avouac, 2000; Avouac, 2003; Yin, 2006; Yeats and Thakur, 2008) (Fig. 1A and B). Understanding the active development of the MFT zone is a key for both unraveling the mechanism of Himalayan growth (Avouac, 2003) and preparing for major earthquake disasters in the future (e.g., Tandon, 1955; Seeber and Armbruster, 1981; Bilham, 1995, 2004; Bilham et al., 1997, 1998, 2001; Bilham and Ambraseys, 2005; Wesnousky et al., 1999; Lavé et al., 2005; Feldl and Bilham, 2006; Szeliga et al., 2010; Kumar et al., 2010). Available GPS data indicate that northeast India at longitude 92°E currently moves at a rate of $\sim$38 mm/yr in the N25°E direction relative to stable Eurasia, whereas northwest India at longitude 76°E moves at a rate of $\sim$35 mm/yr at N11°E relative to stable Eurasia (Zhang et al., 2004).

The MFT in the eastern Himalaya links with the Sumatra subduction zone (e.g., Le Dain et al., 1984; Angelier and Baruah, 2009; Yin, 2010); both tectonic zones have hosted frequent and large ($Ms>8$) magnitude earthquakes (Fig. 1C) (Tandon, 1955; Seeber and Armbruster, 1981; Lay et al., 2005). Because of this, establishing the structural framework and slip rate of the MFT in the far eastern Himalaya is essential to understanding the spatial and temporal evolution of large seismic events along this linked plate-boundary system.

Despite its importance, only a few preliminary studies have focused on the MFT in the eastern Himalaya (e.g., Srivastava and Misra, 2008; Srivastava et al., 2009; Kumar et al., 2010; Chirouze et al., 2012). This situation is in a sharp contrast to the abundant and high-quality studies in the western and central Himalaya across the MFT (e.g., Baker et al., 1988; Jaswal et al., 1997; Powers et al., 1998; Lavé and Avouac, 2000; Kumar et al., 2006) (Fig. 1B). To address this issue, we conduct geologic and geodetic studies to constrain Holocene and GPS slip rates across the MFT in the far eastern Himalaya. Our results indicate that the MFT slip rate in the eastern Himalaya is comparable and possibly higher to that in the central Himalaya but significantly higher than that in the western Himalaya. This observation supports a model that the active growth of the Himalayan

* Corresponding author.
E-mail addresses: yin@ess.ucla.edu, ayin54@gmail.com (A. Yin).

0012-821X/$ - see front matter © 2012 Elsevier B.V. All rights reserved.
http://dx.doi.org/10.1016/j.epsl.2012.09.040

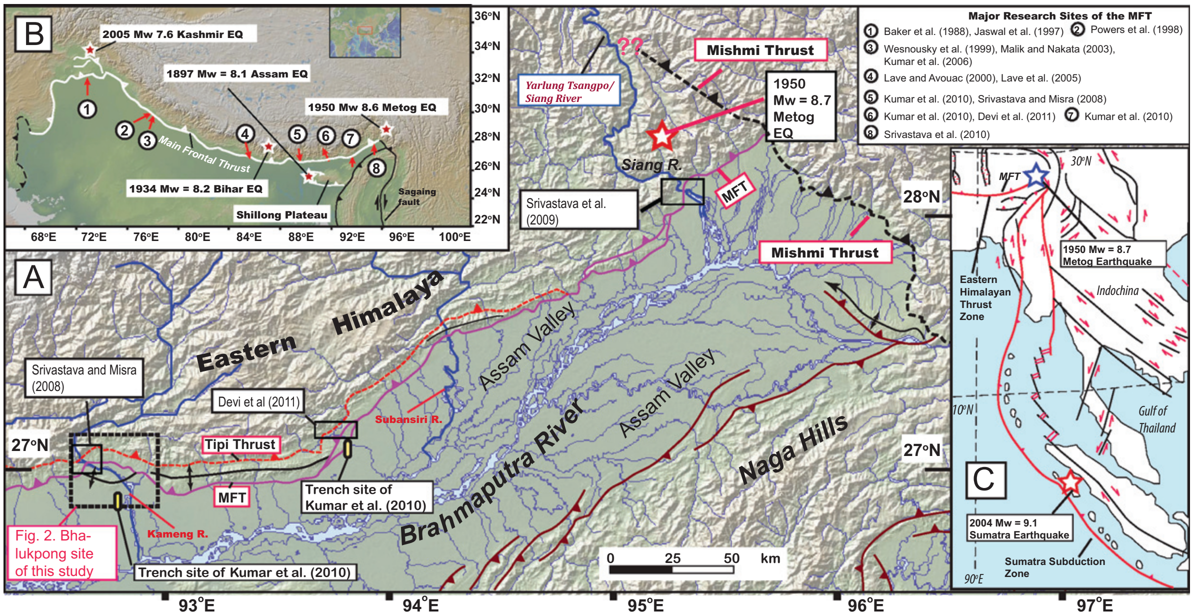

Fig. 1. (A) Major active structures of the eastern Himalayan frontal zone and sites of previous research on Quaternary chronology and active deformation of the MFT zone. Our study area is indicated by the location of Fig. 2. (B) Sites of major historical earthquakes following Chen and Molnar (1977) and Kashmir earthquake following Hussain et al. (2009). Also shown are most relevant studies on the Main Frontal Thrust zone by early workers (see text for detailed description). (C) Tectonic relationship between the eastern Himalayan convergence zone including structures bounding the Shillong plateau and the Sumatra subduction zone.

orogen is mainly controlled by the velocity boundary condition imposed by the India–Asia convergence rather than by gravitational spreading of the Himalayan-Tibetan orogen.

2. Regional geology

2.1. Quaternary slip rates on the MFT

The intense work on the MFT zone in the western and central Himalaya (e.g., Bilham et al., 1998; Lavé and Avouac, 2000; Yeats and Thakur, 2008) may in part be attributed to the better constraints on the ages of Late Cenozoic strata (e.g., Burbank et al., 1996; Ojha et al., 2000, 2009; White et al., 2002). In Pakistan, the shortening rate across Himalayan frontal structures is estimated to be 14 ± 4 mm/yr over the past 5 Ma (Baker et al., 1988; Jaswal et al., 1997) (Fig. 1B). The shortening is mostly concentrated on the MFT, with a minor component partitioned by active faulting in the Himalayan interior (Kaneda et al., 2008; Hussain et al., 2009). In NW India, a Pliocene-Quaternary shortening rate of 14 ± 4 mm/yr was estimated across the MFT and its hanging-wall structures (Powers et al., 1998). The Holocene slip rate of the MFT in NW India is estimated to be 9 ± 3 mm/yr (Wesnousky et al., 1999; Malik and Nakata, 2003; Kumar et al., 2006) (Fig. 1B). Banerjee and Bürgmann (2002) and Ponraj et al. (2011) obtained a GPS shortening rate of ~10–14 mm across NW Indian Himalaya. In Nepal, Lavé and Avouac (2000) established a Holocene slip rate of 21 ± 1.5 mm/yr for the MFT (Fig. 1B), which is similar to the GPS shortening rate across the Nepal Himalaya (Bilham et al., 1997; Jouanne et al., 2004; Ader et al., 2012). Lavé et al. (2005) showed that the MFT in Nepal had ruptured at ~1100 AD along > 240 km length of the MFT. This same rupture event was extended to the eastern Himalaya over a total distance of 600–800 km (Kumar et al., 2010) (Fig. 1B). Although the Holocene MFT slip rate increases eastward from the western to central Himalaya, it is unclear if this trend continues to the eastern Himalaya or an artifact of temporal changes in slip rates at different segments of the Himalaya. An eastward increase in the MFT slip rate would correlate with the eastward increase in the India–Asia convergence rate (e.g., Molnar and Stock, 2009; Copley et al., 2010). This in turn would support the notion that active growth of the Himalaya is mainly controlled by the plate-velocity boundary condition rather than gravitational spreading (see a recent review on this issue by Li and Yin, 2008 and an insight from a simple analog model in Yin and Taylor, 2011).

2.2. Tectonic setting of the eastern Himalaya

Since the pioneering work of Jangpangi (1974) and Gansser (1983), the Bhutan Himalaya has been studied intensely in the past five decades (Ray et al., 1989; Swapp and Hollister, 1991; Ray, 1995; Bhargava, 1995; Edwards et al., 1996; Grujic et al., 1996, 2002, 2006; Davidson et al., 1997; Stüwe and Foster, 2001; Daniel et al., 2003; Tangri et al., 2003; Carosi et al., 2007; Meyer et al., 2006; Richards et al., 2006; Drukpa et al., 2006; Hollister and Grujic, 2006; McQuarrie et al., 2008; Kellett et al., 2009, 2010; Long and McQuarrie, 2010; Long et al., 2011a,b; Chambers et al., 2011). A *minimum* north–south shortening of ~350 km since 22 Ma yields an average *minimum* shortening rate of ~16 mm/yr (McQuarrie et al., 2008). A GPS shortening rate 15–20 mm/yr was obtained by Mukul et al. (2010) across the eastern Himalaya. Although this rate is similar to the long-term minimum shortening rate across the eastern Himalaya, their GPS velocity solution conflicts with other data sets from the same region (see discussion below). Based on 2-yr campaign and data from 8 GPS stations across the Himalayan topographic front and the foreland region directly to the south, Mullick et al. (2009) estimated a shortening of about 11.1 ± 1.5 mm/yr across the area. Their data also reveal puzzling north–south extension as high as 10 mm/yr across a NW-striking fault.

East of Bhutan, Goodwin-Austen (1864), La Touche (1883), MaClaren (1904) and Brown (1912) first studied the Himalayan foothill geology, while Thakur and Jain (1974), Jain et al. (1974), Jangpangi (1974), Acharyya et al. (1975), and Verma and Tandon (1976) established its regional tectonic and stratigraphic framework. Comprehensive reviews of the eastern Himalayan geology can be found in Tripathi et al. (1982), Thakur (1986), Kumar

(1997), Acharyya (1998), Acharyya and Sengupta (1998), and Nandy (2001). Recent work by Yin et al. (2006, 2010a) showed that minimum eastern Himalayan shortening of >500 km had started at or prior to $\sim$25–20 Ma when widespread leucogranites were emplaced and deformed. As the total shortening magnitude was established by bed-length balancing of Proterozoic strata (Yin et al., 2010a), the above estimate may include a component of Cambro-Ordovician crustal shortening, a deformation event well expressed in the nearby Shillong plateau to the south (Yin et al., 2010b).

Although the Shillong plateau had experienced intense early Paleozoic deformation, its high elevation ($\sim$1.5–2 km) is controlled by Late Cenozoic thrusting along its northern and southern edges (Evans, 1964; Gupta and Sen, 1988; Das Gupta and Biswas, 2000; Bilham and England, 2001; Rajendran et al., 2004; Kayal et al., 2006; Biswas et al., 2007; Clark and Bilham, 2008; Yin et al., 2010b). The current north–south GPS shortening rate is 2–5 mm/yr across the plateau (Paul et al., 2001; Jade et al., 2007; Mukul et al., 2010), which is absorbed by plateau-bounding thrusts and by several active left-slip faults in the plateau interior (Kayal and De, 1991; Mitra et al., 2005; Drukpa et al., 2006; Angelier and Baruah, 2009; Yin et al., 2010b). Some of the active structures may have been reactivated from Cretaceous structures, which were formed during the breakup of Gondwana (Gupta and Sen, 1988; Kumar et al., 1996; Srivastava and Sinha, 2004a,b; Srivastava et al., 2005).

3. Geology of the MFT in the study area

Our field area is located near Bhalukpong Village in the foothills of the eastern Himalaya (Fig. 2). Due to the presence of dense forests in a Wild Tiger Nature Reserve, our geologic mapping was conducted mostly along road cuts, deep-cut gullies, trails, and major river banks. The Kameng River, the largest stream in the study area, exposes all major structures and lithologic units along its river banks. Lithologic units and major structures mapped at the well exposed outcrops along the river banks were extrapolated using LANDSAT images laterally to areas covered by trees (Fig. 3A and B).

The weathering-resistant Proterozoic Bomdila Group consisting of phyllite and slate lies in the hanging wall of the Upper Main Boundary Thrust (i.e., MBT-up in Fig. 3A) (Kumar, 1997; Yin, 2010a). Correlative collectively to the Miri, Bichom, Bhareli, and Yamne Formations of Kumar (1997), the Permian strata in the hanging wall of the Lower Main Boundary Thrust (i.e., MBT-up in Fig. 3A) are composed of coal-bearing shale, sandstone, and pebble conglomerate. They form low depressions separating cliff-forming Proterozoic strata to the north and ridge-forming Cenozoic strata to the south (Fig. 3B).

The Cenozoic Dafla, Subansiri, and Kimin Formations of Kumar (1997) below the Lower Main Boundary Thrust crop out continuously along the deep-cut Kameng River. Fission-track dating of detrital apatite and magnetostratigraphic analysis indicates the depositional ages to be 12.2–10.5 Ma for the Dafla Formation, 10.5–2 Ma for the Subansiri Formation, and 2 Ma and younger for the Kimin Formation (Chirouze et al., 2012). The ridge-forming Dafla Formation (Fig. 3B) consists mostly of massive sandstone with minor conglomerate. The Subansiri Formation is also dominated by massive sandstone beds but with a higher proportion of conglomerate. Topographically, the Subansiri Formation is expressed by narrower and broken ridges evident in LANDSAT images; this contrasts with the wider, continuous, and locally cliff-forming ridges of the Dafla Formation (Fig. 3B). The Kimin Formation consists of interbedded sandstone and conglomerate. Its outcrop pattern is characterized by smooth erosional surfaces with fewer gullies (Fig. 3B), indicating its youthfulness since being exposed to erosion.

No Cenozoic growth strata were observed adjacent to major thrusts and folds, as indicated by constant bed thicknesses and similar bedding attitudes in the exposed stratigraphic sections along the banks of the Kameng River (also see Chirouze et al., 2012). The only exception is our observation made in the

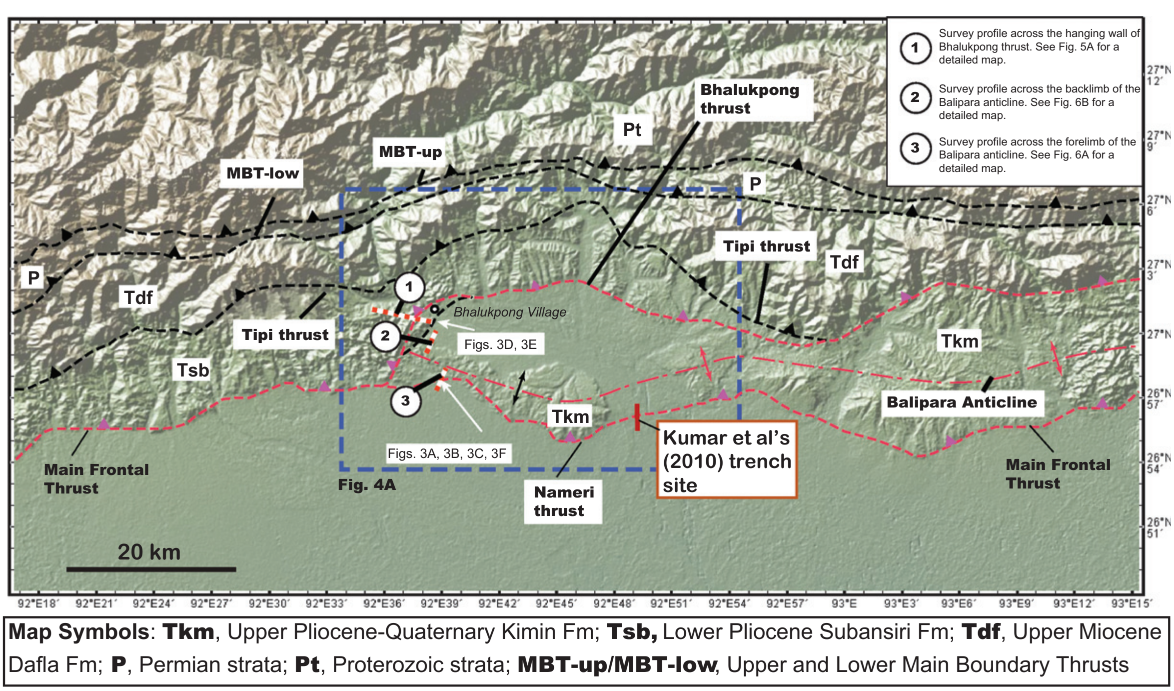

Fig. 2. Major Late Cenozoic structures of the MFT zone in the study area. Red fault and fold-axial traces indicate active structures. Total Station surveying routes by this study are labeled as (1), (2) and (3) (see map legend in the upper right corner). The trench site of Kumar et al. (2010) across the Nameri thrust and the locations of our field photos in Fig. 3A–F are also shown. (For interpretation of the references to color in this figure legend, the reader is referred to the web version of this article.)

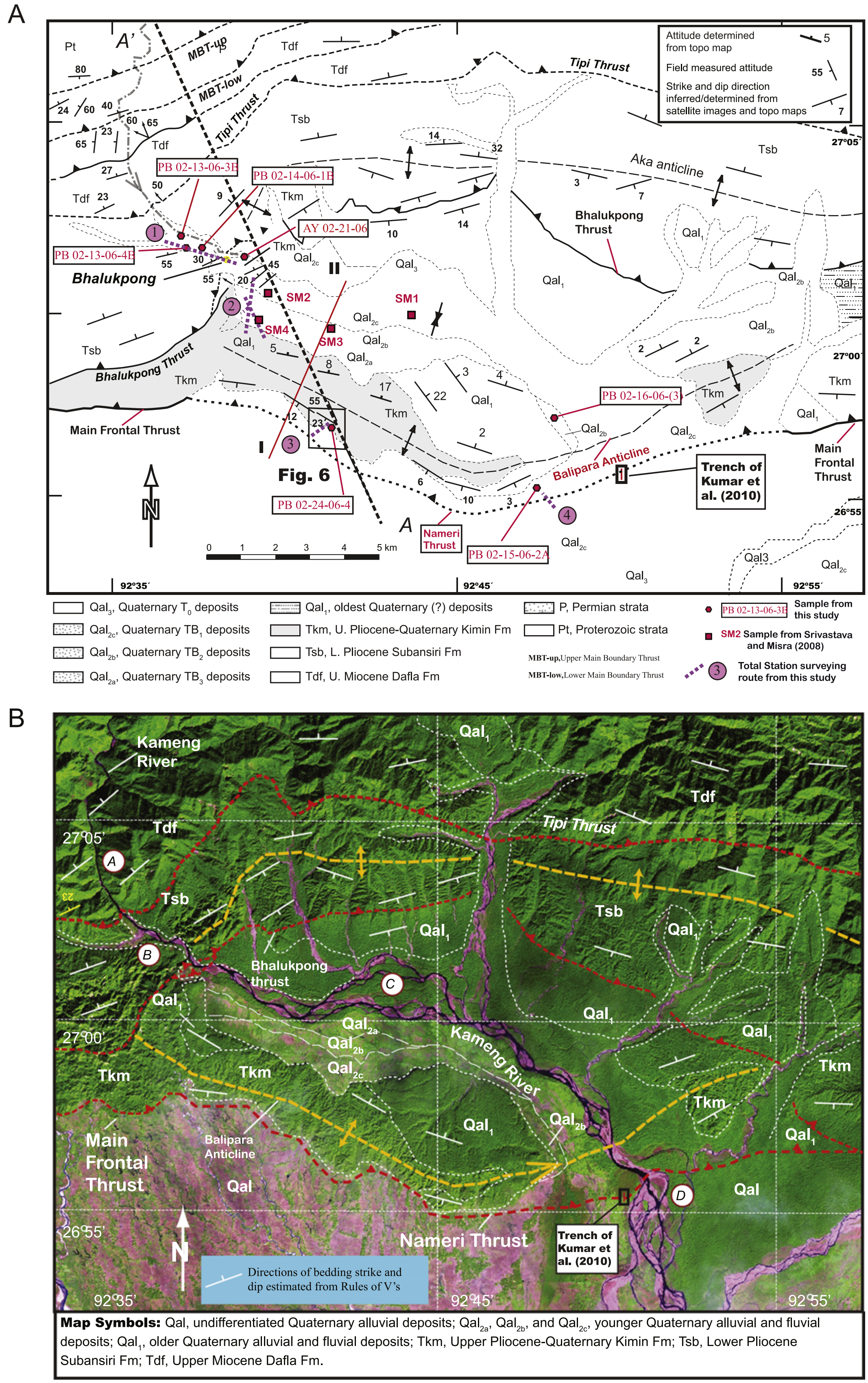

Fig. 3. (A) Geologic map of the study area. See text for detailed mapping procedures. The map shows the locations of age samples, Total Station surveying routes, profile for projection of Total Station data (line I–II), and the geologic cross section (line A–B). Also shown is the trench site location of Kumar et al. (2010) across the Nameri thrust. (B) A LANDSAT image from which major geologic contacts are extrapolated in this study from well-exposed sites mostly along the Kameng River. (C) A balanced cross section across the study area. See text for assumptions and construction procedures. (D) Restored section from cross section shown in (C).

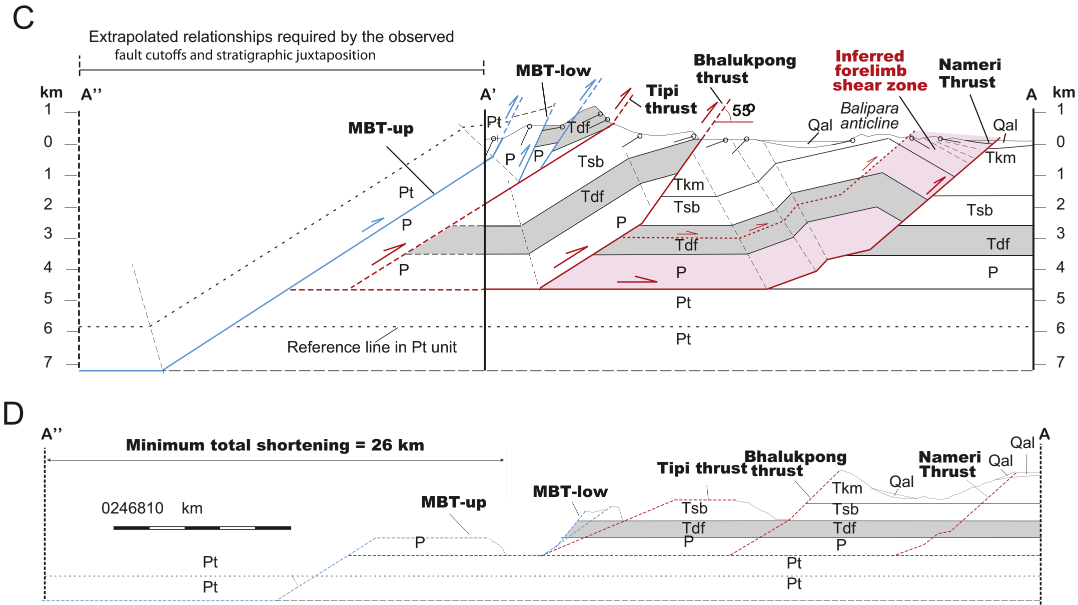

Fig. 3. (*continued*)

upper section of the Kimin Formation across the forelimb of the Balipara anticline (Fig. 4A–C). At this field site bedding dip changes rapidly within a section of <20 m, from $>50^\circ$ to about 20°. This observation suggests very rapid rotation of bedding about horizontal axes during folding. The rotation rate of the forelimb may be estimated if we know the duration of growth–strata sedimentation. According to Chirouze et al. (2012, p. 127), the accumulation rate of the Late Cenozoic sediments in our study area is 420–440 m/Myr. The average rate of 430 m/Myr requires 46.5 ka for 20 m sedimentation, which in turn implies a forelimb rotation rate of $7.88\times10^{-6}\,\mathrm{yr}^{-1}$. As shown below, this rotation rate is remarkably consistent with the Holocene rotational rate we obtained from the age and morphology of the Quaternary terraces we analyzed across the forelimb. Together with the absence of obvious growth strata in the older Cenozoic strata, it appears that Cenozoic deformation in the study area may have started after 2 Ma and possibly at a much younger time given the high stratigraphic position of the growth strata in the Late Pliocene-Quaternary Kimin Formation observed in this study.

Bedding attitudes in Fig. 3A were obtained using three methods: (1) direct field measurements, (2) three-point solutions using 1:50,000 topographic maps superposed over mapped contacts using LANDSAT images, and (3) rough estimates of strikes and dips using the "Rules of V's" from LANDSAT images (Fig. 3A). Our geologic map also incorporates the early work of Kumar (1997) who mapped the Tipi thrust, the work of Kumar et al. (2010) who mapped the Nameri thrust, and the more recent work of Yin et al. (2010a) who first mapped the Bhalukpong thrust (Fig. 3A).

A geologic cross section is constructed across the study area using the dip-domain method of Suppe (1983) (Fig. 3C). We assign a minimum depth of 4.8 km to the decollement at the base of Permian strata, which are the oldest exposed unit in the MBT footwall. Restoration of the section requires a minimum shortening of 26 km (Fig. 3D). The minimum estimate comes from the fact that the hanging-wall cutoffs of the MBT-up, MBT-low, and the Nameri thrust are all eroded (Fig. 3C and D). If the thrust belt between the MBT-up in the north and the Nameri thrust in the south across our study area were initiated during the deposition of the upper Kimin Formation, it implies a minimum shortening rate of 13 mm/yr.

4. River terraces and channel geometry

4.1. Strath terraces in the hanging wall of the Bhalukpong thrust

The Bhalukpong thrust splits into two splays across the Kameng River (Figs. 2 and 3A). The northern trace defining a sharp topographic front *does not cut* Quaternary deposits, whereas the southern trace places the Subansiri Formation directly over Quaternary gravel and sand. This southern trace also displays a prominent fault scarp (Fig. 4D). A flight of four parallel strath terraces were mapped onto 1:50,000 Indian topographic maps in the hanging wall of the Bhalukpong thrust zone along the Kameng River (Fig. 5A and B). The inferred elevations of the terrace surfaces are interpreted from extrapolating from the nearby contour lines, which have a 40-m interval. For a ground surface that is perfectly planar between two contour lines, their elevation distribution can be established accurately using a linear interpolation. For a ground surface that is concave upwards or downwards, the linear extrapolation would lead to overestimates and underestimates of the true terrace-surface elevations. Based on comparison against our Total Station surveying results (see below), we found that the uncertainty can be as high as ±10 m across steeply cut river banks but as low as ±2 m when dealing with regions that are flat.

We also surveyed the tread-elevation profiles using a Total Station with sub-cm accuracy (Fig. 5C). The surveyed treads, particularly the older terrace surfaces, display vertical undulations up to 1–2 m due to fluvial erosion and colluvium deposition. Because of this, we assigned ±2 m for each Total Station survey point in our plots (Fig. 5C). For the young terrace surfaces this undulation is likely within ±1 m.

The terrace deposits in the hanging wall of the Bhalukpong thrust are typically 3–10 m thick and contain cobble and boulder below and sand and silt above. The contacts between the two types of deposits are sharp (e.g., Fig. 4A).

4.2. Quaternary age dating and interpretations

We obtained radiocarbon and optically stimulated luminescence (OSL) dates from the Keck-CCAMS facility at University of

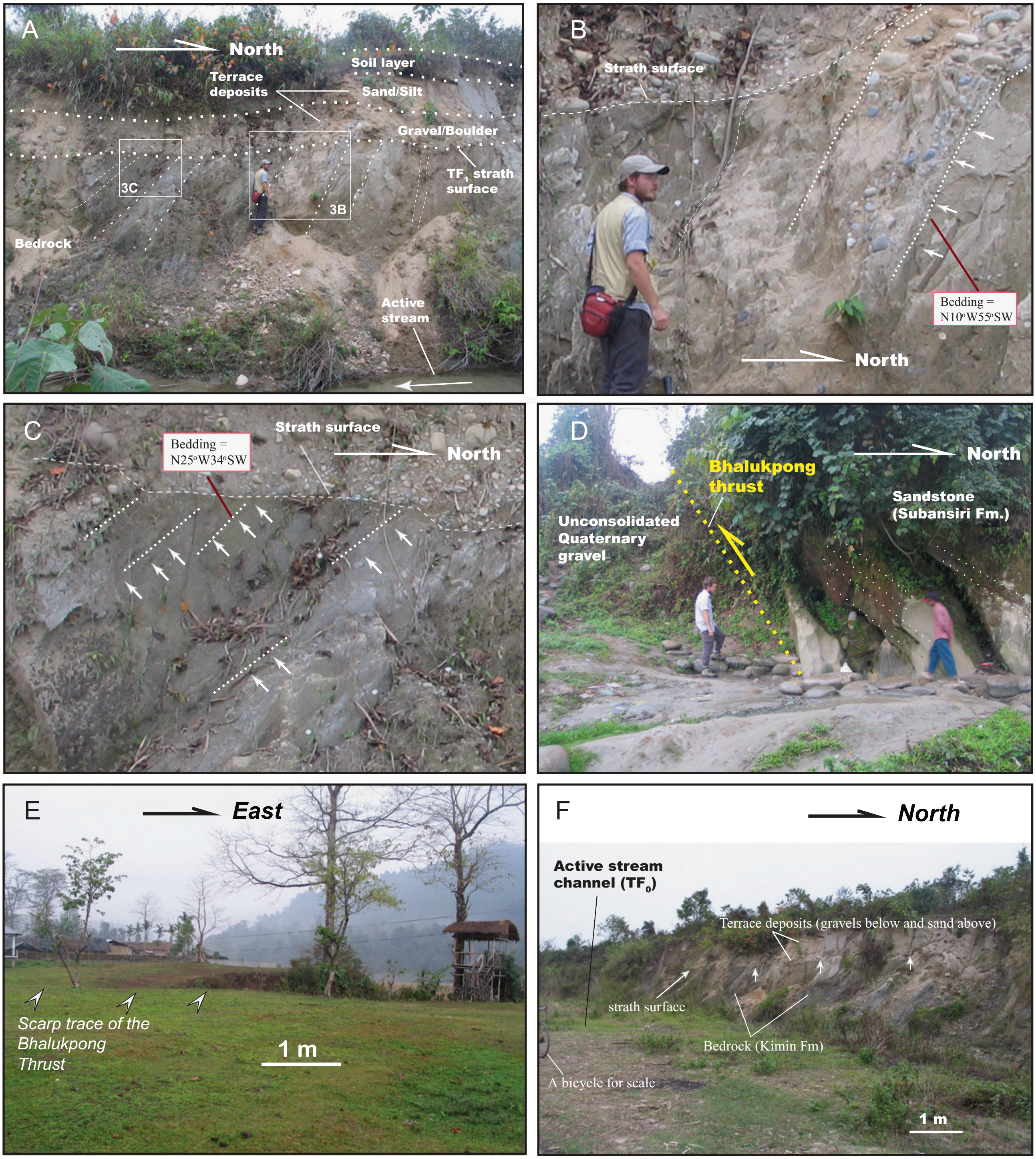

Fig. 4. (A) View of TF_1 terrace deposits, strath surface, and underlying bedrock. The terrace deposits consist of a ~50 cm to 80 cm thick layer of gravel and boulder below and a 60–70 cm thick layer of sand and silt. The contact between the two types of sediments is sharply defined. Bedrock below strath surface displays rapid change in bedding attitude, interpreted as representing growth strata. See Fig. 2 for location. Also shown are locations of close-up views. (B) Close-up view of steeply dipping beds in the northern part of the stream-cut section shown in (A). (C) Close-up view of shallowly dipping beds in the southern part of the stream-cut section in Fig. 3A. (D) Exposure of the Bhalukpong thrust at a cut-bank of the Kameng River. Note that the fault dips steeply to the north. Note that the cutoff angle between hanging-wall beds and the thrust is about 30°, which requires that the footwall ramp of the thrust dips at this angle if the beds have not been rotated. (E) Relic of a fault scarp along the trace of the Bhalukpong thrust. The preserved scarp height is about 70–100 cm. (F) Photo of TF_1 strath terrace along the same valley where photo shown in (A) was taken. This photo is located farther downstream in the valley near the mouth of the active stream as it exits the anticlinal hills.

California, Irvine, and the IIRMES Lab of California State University at Long Beach, respectively (Table 1). As our dated charcoal fragments are detrital, their dates represent the oldest possible ages of sedimentation when the detrital charcoal grains were laid down. For OSL dating, one needs to keep in mind that the effectiveness of the technique depends on whether the dated grains are completely bleached. The degree of bleaching of dated quartz grains is controlled by its depositional environment (Rhodes, 2011). That is, more effective bleaching is achieved by repeated and/or lengthy light exposure (e.g., beaches, dunes)

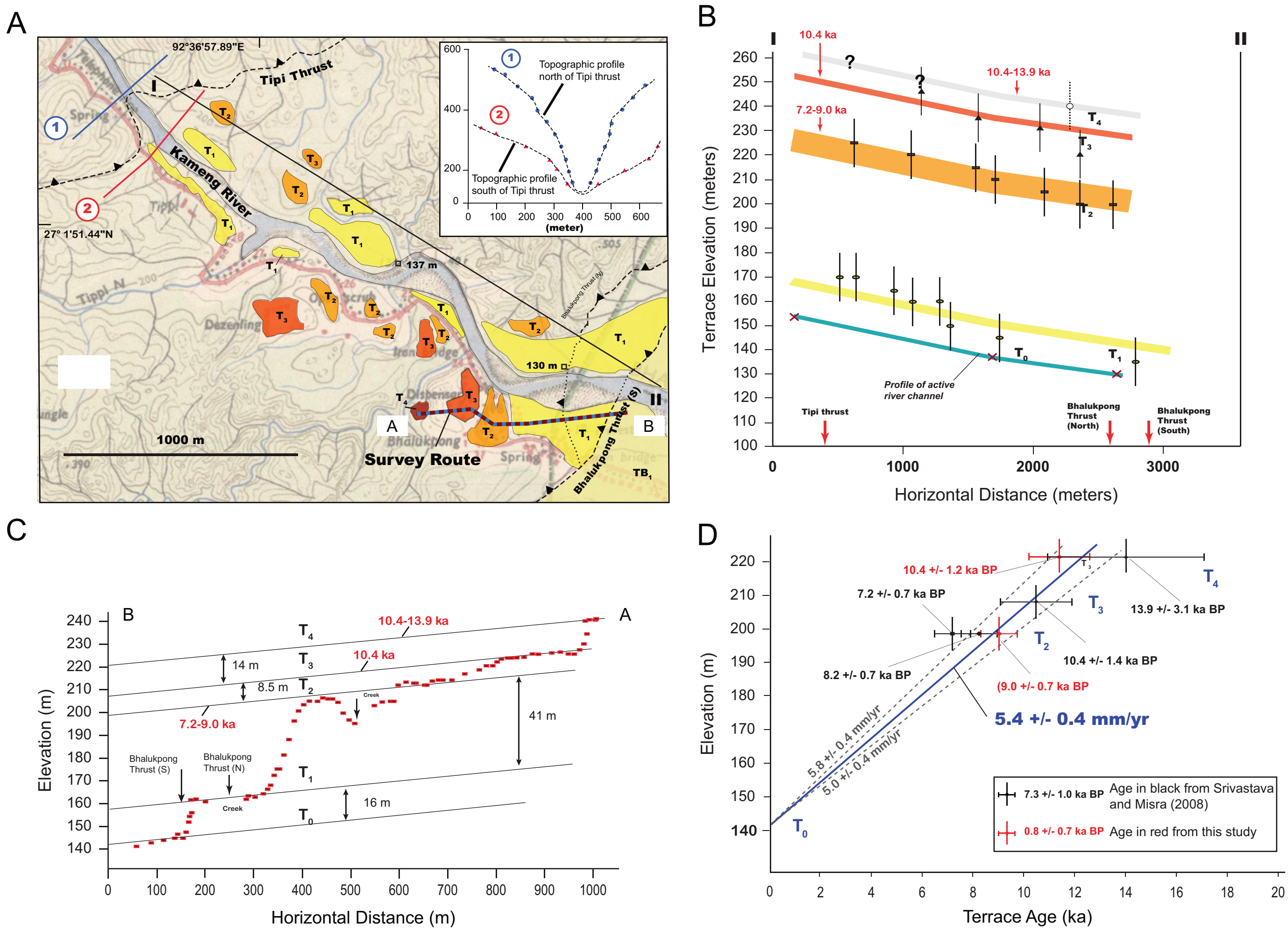

Fig. 5. (A) Distribution of terraces and the location of elevation profile across the hanging wall of the Bhalukpong thrust. See "Survey Route 1" in Fig. 2 for location. (B) Elevation profiles of terrace surfaces estimated from the use of 1:50,000 topographic maps. (C) Elevation of profiles of terrace treads in the hanging wall of the Bhalukpong thrust determined by Total Station surveying. (D) Incision rate of the Bhalukpong thrust hanging wall based on the elevation profiles and ages of Holocene terraces. See text for details.

while incomplete bleaching occurs in environments with little light exposure (e.g., debris flows, moraine, and flood deposits). Environmental histories of dated grains also matter (Rhodes, 2011): grains recently eroded from bedrock typically bleach more slowly than those with an extended residence at the surface. As our OSL samples were all collected from mountain-stream-channel deposits, it is most likely that the dated grains by the OSL method have not been completely bleached. As a result, the obtained ages should be regarded as lower bounds for true depositional ages (Rhodes, 2011). Because of this issue, when the same sediments were dated by both the radiometric and OSL methods, we use the radiometric ages as they are not affected by the bleaching issue. Because both radiometric dating of detrital charcoals and OSL dating of incompletely bleached grains place minimum ages of sedimentation, the inferred slip rates discussed below are likely to represent lower-bound values.

Our dating strategy was to collect sand samples of fine-grained sand at the uppermost horizon of the gravel and boulder layer and/or at the lowest horizon of the sand–silt layer. Following Lavé and Avouac (2000), we interpret the upper layer of sand and silt as a result of over-bank deposits on top of entrenchment of strath terraces, whereas the lower layer of gravel and boulders formed as a result of deposition when the strath surfaces were still parts of active stream channels. As the terrace treads are parallel to one another and to the active Kameng River, we interpret that the longitudinal treads represent the past channel profiles. The parallel relationship also suggests that the river has maintained a constant equilibrium profile during the formation of the observed terraces. This interpretation implies that the channel response time to tectonic and climatic perturbations is much shorter than the formation time of individual terraces, which is characteristic for humid regions with high seasonality (Bull, 1991). A consequence of this interpretation is that all the surveyed terraces were developed synchronously. Note that Srivastava and Misra (2008) obtained OSL ages for all four terraces in the hanging wall of the Bhalukpong thrust that we mapped. Their data are also summarized in Table 1.

4.3. River terraces across the growing Balipara anticline

The Balipara anticline is bounded by the Bhalukpong thrust zone in the north and the Nameri thrust in the south. The backlimb beds dip 8–15° near the fold hinge and 20–45° farther to the north (Fig. 3A). Due to poor access and poor outcrop conditions, few bedding attitudes were obtained across the forelimb (Fig. 2).

Three terraces across the backlimb (TB_1, TB_2 and TB_3) and three terraces across the forelimb were mapped in this study (TF_1, TF_2 and TF_3) (Fig. 6A and B). The backlimb terrace TB_1 can be further divided into two sub-surfaces: TB_{1a} and TB_{1b}. The TB_{1a} surface is exposed along the two sides of Kameng River and is mostly covered by forests. The strath surface of TB_{1a} has a gentler

Table 1
Age summary of quaternary units.

Sample numbers	GPS location	Method	Ages	Unit/position
(1) BT HW				
PB 02-14-06-(1)B	N27°01′04.02″ E92°38′11.94″	OSL dating	8986.8 ± 923.6 yr BP	T_2 (BT hanging wall)
SM-2	N27°00′53.60″ E92°38′16.30″	OSL dating	(1) 7.2 ± 0.7 ka BP (2) 8.2 ± 0.7 ka BP	T_2 (BT hanging wall)
SM-3	N27°01′00.30″ E92°38′09.20″	OSL dating	10.4 ± 1.4 ka BP	T_3 (BT hanging wall)
PB 02-13-06-(3)B	N27°01′04.56″ E92°38′02.94″	OSL dating	4084.2 ± 530.4 yr BP	Talus on top of T_2 (BT hanging wall)
PB 02-13-06-(4)B	N27°00′58.68″ E92°38′00.84″	OSL dating	10,385.3 ± 1230.6 yr BP	T_4 (BT hanging wall)
SM-4	N27°00′58.20″ E92°37′59.10″	OSL dating	13.9 ± 3.1 ka BP	T_4 (BT hanging wall)
(2) BA backlimb				
AY 02-21-06	N27°00′48.24″ E92°38′48.06″	Radiocarbon dating	618 ± 37 yr BP	TB_{1a} (backlimb of Balipara anticline)
SM-1	N27°01′02.40″ E92°38′48.90″	OSL dating	7.3 ± 1.0 ka BP	TB_{1b} (backlimb of Balipara anticline)
PB 02-16-06-(3)A	N26°56′29.17″ E92°47′40.71″	Radiocarbon dating	(1) 922 ± 11 yr BP (2) 906 ± 28 yr BP	Soil layer on top of TB_2 (backlimb of Balipara anticline)
PB 02-16-06-(3)C	N26°56′29.17″ E92°47′40.71″	OSL dating	6094 ± 719.6 yr BP	TB_2 (backlimb of Balipara anticline)
PB 02-16-06-(3)B	N26°56′29.17″ E92°47′40.71″	OSL dating	16,347.5 ± 2584.5 yr BP	TB_2 (backlimb of Balipara anticline)
(3) BA forelimb				
PB 02-15-06-(2)	N26°59.718′ E92°47.696′	Radiocarbon dating	(1) 1237 ± 29 yr BP (2) 3721 ± 38 yr BP	TF_3 (forelimb of Balipara anticline)
PB 02-24-06-(4)	N26°56′38.04″ E92°41′37.74″	Radiocarbon dating	(1) 883 ± 38 yr BP (2) 883 ± 38 yr BP	TF_2 (forelimb of Balipara anticline)

BT, Bhalukpong thrust; BA, Balipara anticline; HW, hanging wall; PB samples are from this study while SM samples are from Srivastava and Misra (2008).

north-dipping slope than the nearby active Kameng River. As a result, its northernmost part is buried below Quaternary gravels immediately below the Bhalukpong thrust (Fig. 4D) whereas its southern part emerges above the stream channel of the Kameng River along which bedding of the Kimin Formation can be observed and measured directly (Fig. 3A). The relationship between the TB_{1a} strath terrace and the Kameng River channel is similar to that shown in Fig. 7C.

Directly against the Kameng River, the TB_{1a} strath surface is about 2 m above the Kameng stream channel, whereas its top surface is about 3.5–4.5 m above the stream channel. The TB_{1b} terrace surface is extensively farmed and can be accessed easily by numerous roads. Our Total Station surveying indicates that this and all other backlimb terrace surfaces are parallel. This is in contrast to the observation based on Total Station surveying across the forelimb where the terraces converge towards the southern edge of the Balipara Hills (Fig. 6C). The converging relationship across the forelimb is well displayed by the best preserved and most continuous TF_1 tread and our Total Station data obtained from the TF_3 surface (Fig. 6A and C). The convergence of the TF_1 strath surface towards the TF_0 at the mouth of an active stream channel can be observed directly in the field, which is expressed by an upstream increase in the height of the TF_1 strath surface (Fig. 4A and F).

Although the survey terrace profiles across the forelimb converge to each other, they do not intersect at one point at the base of the surveyed hill slope. The range of scattering as allowed by the distribution and uncertainty of the data points is ±75 m when all the surveyed profiles are projected onto a horizontal plane passing the base of the slope. The data scatter may be attributed to (1) projection of non-planar terrace surfaces, (2) projection of a curvilinear hinge zone around which the terrace surfaces were rotated, and (3) southward motion on the Nameri thrust. Regardless of the causes for the terrace profiles not intersecting precisely at a point, the fact that the terrace slope increases with age can be attributed to forelimb rotation during folding, although the hinge of rotation may have migrated with time laterally (Fig. 6C).

Sample AY 02-21-06 (see Fig. 3A for location) was collected from a fine-grained sand layer immediately above a 3–4 m thick boulder layer exposed at along the Kameng River below the Bhalukpong thrust (Fig. 4D). This sample yields a ^{14}C date of 618 ± 37 yr BP. The detrital nature of the dated charcoal grains places 618 ± 37 yr BP as the maximum age of deposition.

We obtained three samples from terrace deposits of TB_2 in a 4 m thick section. Samples PB 02-16-06-(3A) and PB 02-16-06-(3B) were collected from two fine-grained sand in the middle and upper parts of a gravel layer; the samples yield OSL ages of 16.4 ± 2.6 ka BP and 6.1 ± 0.7 ka BP, respectively. We interpret these ages to represent the times when channel deposition was active. Sample PB 02-16-06-(3)C was collected at the base of a sand–silt layer, which yields two ^{14}C age clusters at 922 ± 11 yr BP and 908 ± 28 yr BP. We interpret these dates to represent the onset of strath entrenchment induced by stream incision. As the dated charcoal grains are detrital, the above dates represent the maximum ages of terrace deposition. An OSL date of 7.3 ± 1.0 ka BP was obtained by Srivastava and Misra (2008) from TB_{1b} deposits. In light of our OSL dates with clearly defined

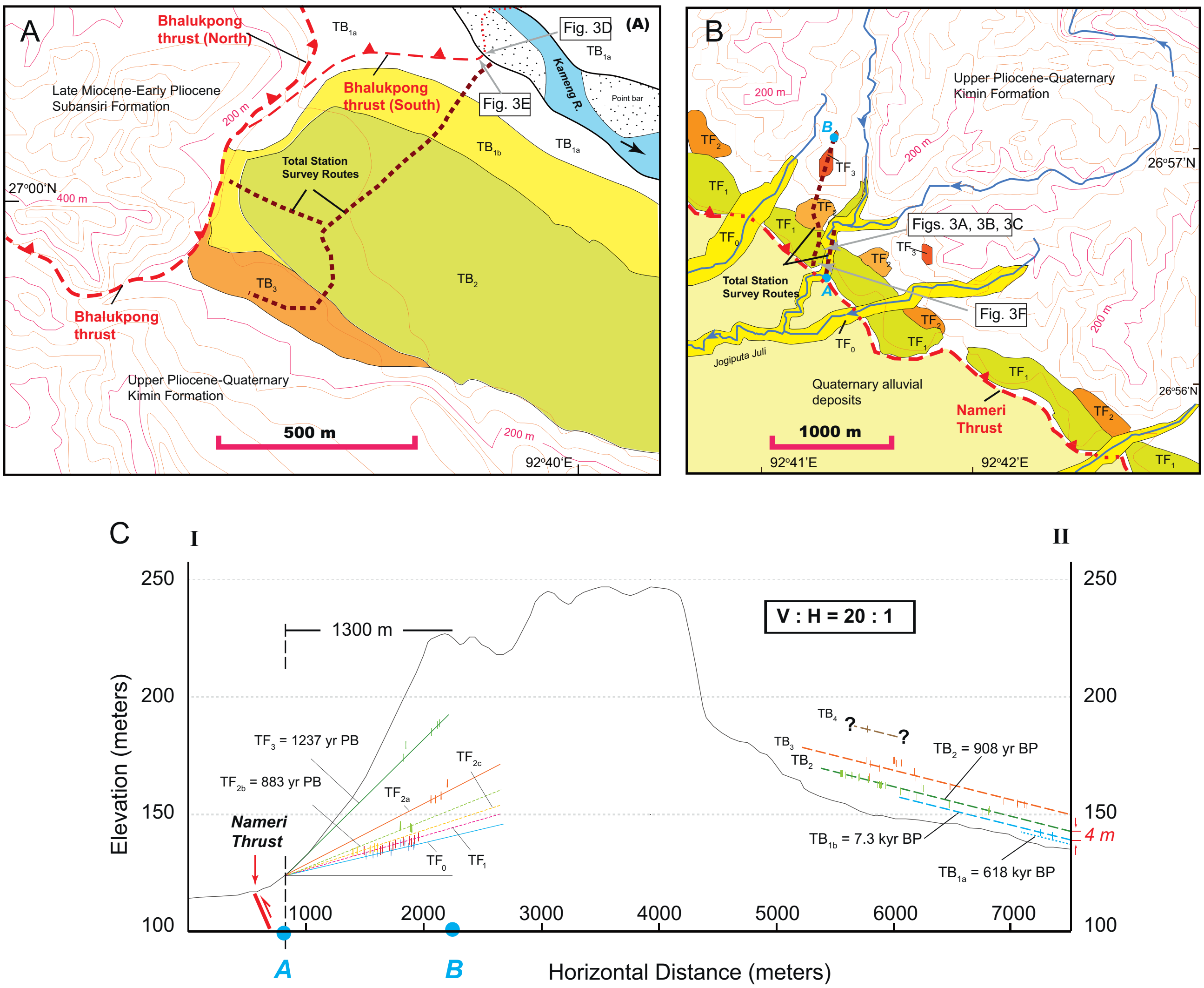

Fig. 6. (A) Distribution of major Quaternary terrace units across the backlimb of the Balipara anticline. See "Survey Route 2" in Fig. 2 for location. Also shown are locations of field photos in Fig. 4D and E. (B) Distribution of major Quaternary terrace units across the forelimb of the Balipara anticline. See "Survey Route 3" in Fig. 2 for location. Also shown are locations of field photos in Fig. 4A, B, C and F. (C) Elevation profiles of terrace treads determined by Total Station surveying across the Balipara anticline. See Figs. 2 and 3 for locations of survey routes.

stratigraphic relationships on timing of channel abandonment, the older OSL age obtained by Srivastava and Misra (2008) may represent the time when the stream deposition of TB_2 sediments was still active.

We obtained age constraints from two forelimb terraces. Sample PB 02-24-06-(4) from TF_2 deposits yields two radiocarbon ages clusters at 912 ± 11 yr BP and 883 ± 38 yr BP, whereas sample PB 02-15-06-(2) from TF_3 deposits yields two radiocarbon age clusters at 3721 ± 38 yr BP and 1237 ± 29 yr BP. As dated charcoal grains are detrital, the younger ages of 883 yr BP and 1237 yr BP are taken to represent the lower age bounds of TF_2 and TF_3 sediments, respectively.

4.4. Relationship between channel geometry and Quaternary fault activities

Channel geometry of the Kameng River changes noticeably as it traverses major Cenozoic structures in the study area. In the hanging wall of the Tipi thrust, the channel is nearly straight and forms a deep-cut gorge. The channel is characterized by lacking point-bar deposits (segment *A* in Fig. 3B). South of the Tipi thrust the Kameng River displays meandering channel geometry (segment *B* in Fig. 3B) with well-developed point bars. The river valley is expressed by gentler channel-wall slopes than those north of the Tipi thrust (see topographic profiles shown in Fig. 5A). The Kameng River doubles its channel width immediately across the Bhalukpong thrust and displays dominantly braided-channel networks (segment *C* in Fig. 3B). The braided river channel increases its width sharply southward across the Nameri thrust (segment *D* in Fig. 3C). As the Bhalukpong and Nameri thrusts can be shown to be active, as both cut Quaternary deposits, the abrupt change in channel morphology across them can be confidently correlated to active tectonics (e.g., Bull, 1991; Lavé and Avouac, 2001; Duvall et al., 2004; Turowski et al., 2006, 2009; Amos and Burbank, 2007). This correlation for the Tipi thrust is not obvious, as the abrupt change in channel morphology correlates to different lithology across the fault: the more weathering-resistant Dafla Formation in the hanging wall and less weathering-resistant Subansiri Formation in the hanging wall (Fig. 3B). Lithology-controlled changes in channel geometry without the influence of tectonics have been documented widely around the world (Cook et al., 2009; Roberts and White, 2010). From our analysis of LANDSAT images, the trace of the active Bhalukpong thrust appears to merge with the Tipi thrust along

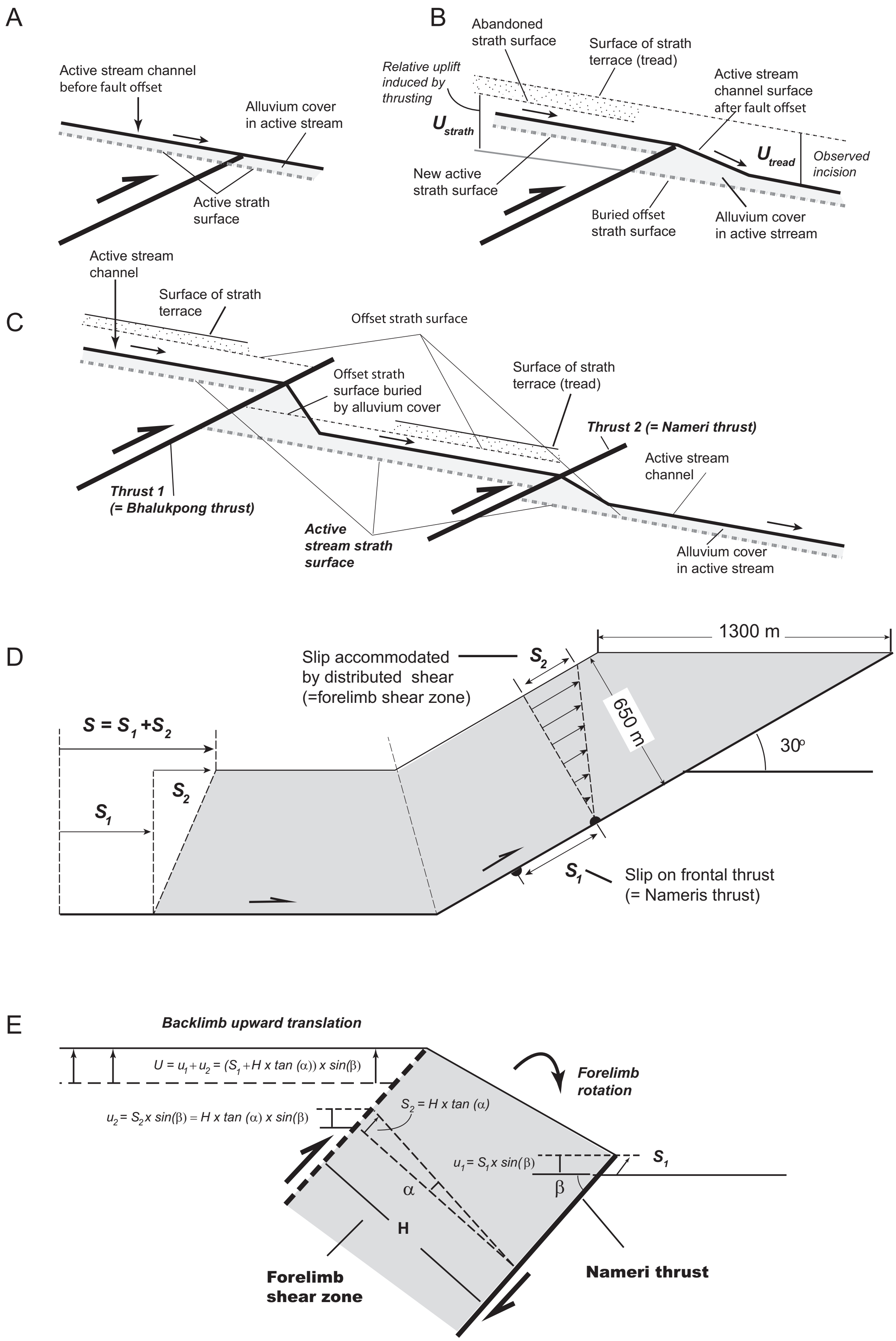

Fig. 7. (A) and (B) show the relationship between the thrust offset and measured river incision in the thrust hanging wall. Sedimentation directly below the active thrust buries the offset channel. (C) Offset a reference strath terrace by multiple thrusts. (D) Relationship between total slip along the basal decollement, slip on the frontal thrust (Nameri thrust), and forelimb shear zone parallel to the Nameri thrust. (E) Relationship among backlimb incision, motion on the frontal thrust (i.e., the Nameri thrust), and simple-shear deformation across the forelimb shear zone that is assumed to be parallel to the Nameri thrust. See text for details.

strike to the east, requiring that some portions of the Tipi thrust may be active. Indeed, Devi et al. (2011) argued that the Tipi thrust is active at a site about 100 km east of our study area (Fig. 1A).

5. Quaternary shortening rate across the MFT zone

5.1. Slip rate along the Bhalukong thrust

Assuming a constant incision rate during the development of terraces in the hanging wall of the Bhalukpong thrust, we obtain an incision rate of 5.4 ± 0.4 mm/yr (Fig. 5D). Because thrusting along the Bhalukpong thrust may lead to burial of the offset footwall channel (Fig. 7A and B), the hanging-wall incision rate can only be used to constrain a minimum rate of tectonic uplift and the related slip rate along the underlying thrust. This scenario also applies to the presence of multiple active thrusts (Fig. 7C). Although the Bhalukpong thrust dips 55° at the surface (Fig. 3A), its cutoff angle to the hanging-wall bedding is about 22–30° (Fig. 4D). This observation suggests that the dip of the thrust across its footwall ramp must dip at 22–30°, assuming that it has not been modified as shown in our cross section (Fig. 3C). Using the functional form of $\dot{S} = \left(\dot{I}/\sin\alpha\right)$, where $\dot{S}$ is the slip rate on the fault, $\dot{I}$ is the vertical incision rate, and α is the dip angle of the fault, we obtain an uncertainty of the fault slip rate due to a variation of fault dip angle to be $\sigma_{\dot{S}} \le \left|\left(\partial\dot{S}/\partial\alpha\right)\sigma_\alpha\right| + \left|\left(\partial\dot{S}/\partial\dot{I}\right)\sigma_{\dot{I}}\right| = \left|\dot{I}\left(\cos\alpha/\sin^2\alpha\right)\sigma_\alpha\right| + \left|(\sigma_{\dot{I}}/\sin\alpha)\right|$. We assume that the variations of fault dip and incision rate $40 \pm 15°$ and 5.4 ± 0.4 mm/yr. Thus, for $\alpha = 40°$, $\sigma_\alpha = 10°$, $I = 5.4$ mm/yr, and $\sigma_{\dot{I}} = 0.4$, we obtain an uncertainty for the estimated slip rate of 8.4 mm/yr to be $\sigma_{\dot{S}} \le 2.37$ mm/yr, or $\dot{S} = 8.4 \pm 2.4$ mm/yr.

Note that the above estimated slip on the Bhalukpong thrust should represent a minimum value. This is because the reference surface for fault offset is the strath surface (i.e., the top of the river bedrock), not the top surface of channel gravel deposits used in the above offset estimates. As shown in Fig. 3D the footwall deposits directly below the Bhalukpong thrust are unconsolidated Quaternary gravels where no strath surface is exposed. In fact, the footwall strath surface does not emerge in the active river channel for >1 km downstream from the trace of the Bhalukpong fault (see Fig. 2A). On the other hand, the offset in the hanging wall is measured by exhumed strath surfaces. Thus, the vertical distance between the active channel surface overlain by Quaternary sediments and the hanging-wall strath surfaces represents minimal vertical offset caused by motion on the Bhalukpong thrust. The above stated field relationship is illustrated in Fig. 7C.

5.2. Shortening rate across the Balipara anticline

To explain progressive steepening of the forelimb terraces and parallel relationship of the backlimb terraces (Fig. 6C), we propose a simple model in which the formation of the Balipara anticline was accommodated by distributed shear across the forelimb of the fold together with motion on the Nameri thrust (Fig. 7D and E). As we have no controls on the deformation field of the forelimb at depth, the geometry of the inferred forelimb shear zone is not constrained. The simplest assumption is that the shear zone directly above the Nameri thrust is part of the Nameri fault zone. That is, the shear zone is bounded by the Nameri thrust below and a parallel plane above (Fig. 7D). According to our simple model, the tectonic uplift rate of the backlimb $\left(\dot{U}\right)$ may be related to the slip rate $\left(\dot{S}_1\right)$ on the Nameri thrust and the shear–strain rate $(\dot{\gamma})$ across the forelimb by the following relationship (Fig. 7E):

$$\dot{U} = [\dot{S}_1 + \dot{S}_2]\sin(\beta) = [\dot{S}_1 + H\dot{\gamma}]\sin(\beta) \tag{1}$$

where β is the dip angle of the Nameri thrust (which is assumed to be parallel to the simple-shear zone across the forelimb), $\dot{S}_2$ is the slip rate across the forelimb shear zone, and H is the thickness of the forelimb shear zone. The forelimb shear–strain rate can be obtained from the elevation profiles and ages of the forelimb terraces by

$$\dot{\gamma} = \frac{\tan(\theta_{i+1} - \theta_i)}{(t_{i+1} - t_i)} \tag{2}$$

where θ_{i+1} and θ_i are the slopes of forelimb terrace surfaces developed at stages $(i+1)$ and i, and t_{i+1} and t_i are the ages of terraces.

To determine the tectonic uplift rate for the backlimb of the Balipara anticline, we use the ages and elevation profiles of the backlimb terraces to estimate the incision rate. Similar to the situation for the terrace development in the hanging wall of the Bhalukpong thrust, the incision rate of the backlimb also represents a minimum value of the tectonic uplift rate because sedimentation in the footwall of the Nameri thrust may have buried the offset channels. As mentioned above, detrital charcoal collected from terrace deposits of TB_{1a} yields a maximum age of deposition at $\sim$ 618 yr BP (e.g., site AY 02-21-06 in Fig. 3A). The terrace surface lies about 3.5 m above the modern stream channel of the Kameng River (Fig. 4D), which requires a minimum incision rate of 5.7 mm/yr since the onset of its entrenchment. Based on our Total Station surveying, the tread of terrace TB_2 lies 4 m above terrace surface $TB_{1b,}$ which is in turn $\sim$1 m above TB_{1a} (Fig. 6C). Using the youngest radiocarbon age of 908 yr BP for the age of TB_2 formation, we obtain a minimum incision rate of 9.4 mm/yr since the start of its entrenchment. Averaging the two estimates yields an incision rate of 7.5 ± 1.9 mm/yr. According to Kumar et al. (2010), the Nameri thrust dips from 8° to 30° at the surface. To be conservative for our slip rate estimates, we took a dip angle of 30° for the Nameri thrust and the bounding planes of the inferred forelimb shear zone. This assumed thrust and shear-zone dip requires a minimum total slip rate of 15 ± 3.8 mm/yr along the decollement below the Nameri thrust and the Balipara anticline.

The horizontal distance of our Total Station surveying profile across the forelimb is 1300 m, along which tilted terrace surfaces were observed (Fig. 6C). A 30° dip of the shear zone requires a minimum thickness of 650 m. The shear–strain rate can be calculated from the observed magnitude of angular rotation of TF_{2b} and TF_3 with respect to TF_0 and their ages. We take the youngest charcoal ages of 883 yr B.P. and 1237 yr B.P. for the maximum ages of the two terraces. The rotation of terraces can be determined from the gradients of TF_0, TF_{2b}, and TF_3 at 0.01143, 0.01714, and 0.04286 from the elevation profiles (Fig. 6C). The above information yields a minimum rotation rate (=minimum shear–strain rate) of 6.47×10^{-6} yr^{-1} for TF_3 and a minimum rotation rate of 2.54×10^{-5} yr^{-1} for TF_{2b} relative to TF_0. Note that the above rotation rate is remarkably similar to the rotation rate of 7.88×10^{-6} yr^{-1} we derived from the growth–strata relationship across the forelimb along the same valley. Using the minimum shear-zone thickness of 650 m and the average of the two minimum rotation/shear–strain rates, we obtain a minimum slip rate of 9.8 ± 6.8 mm/yr across the surface of the inferred forelimb shear zone. As the minimum total slip rate is $\sim$15 mm/yr and the minimum shortening rate across the forelimb shear zone is $\sim$10 mm/yr when removing the uncertainties, we obtain a roughly estimated Holocene slip rate of $\sim$5 mm/yr for the Nameri thrust.

6. Discussion

The estimated *minimum* slip rate on the Bhalukpong thrust is 8.4 ± 2.4 mm/yr, whereas the estimated *minimum* slip rate along the same decollement below the Balipara fold and the Nameri thrust is 15 ± 3.8 mm/yr. This yields a *minimum* total slip rate of 23.4 ± 6.2 mm/yr along the MFT-zone decollement (Fig. 3C). Note that the above estimates critically depend on the deep crustal structures inferred from construction of a balanced cross section, which is a possible but non-unique solution. This uncertainty cannot be evaluated quantitatively without subsurface data such as seismic reflection profiles and drill-hole controls on the thickness and position of stratigraphic units and fault positions. With this uncertainty in mind, our estimated slip rate along the MFT-zone decollement in the eastern Himalaya is similar in magnitude to and potentially greater than the estimated Holocene slip rate of 21 ± 1.5 mm/yr for the MFT in the central Himalaya (Lavé and Avouac, 2000). However, our estimated Holocene shortening rate in the eastern Himalaya is significantly higher than the Holocene shortening rate of 9 ± 3 mm/yr for the MFT in the western Himalaya (Wesnousky et al., 1999; Malik and Nakata, 2003; Kumar et al., 2006). Our estimated MFT slip rate together with the existing MFT slip-rate estimates from the western and central Himalaya indicates that the active deformation of the Himalayan orogen correlates closely to the eastward increase in the Indo-Asian convergence rate (e.g., Molnar and Stock, 2009).

We obtain a GPS velocity field across the Himalayan orogen and southern Tibet referenced to the stable interior of the Indian craton (Fig. 8). Data used in our plot are from Gan et al. (2007), Jade et al. (2007) and Ader et al. (2012). Although the work of Mukul et al. (2010) covers the region of our interests, we decided not to include their GPS data as we found their data analysis and processing problematic. First, some of their sites in the figures and the data table do not match one another. Second, we are unable to obtain a reliable reference from their dataset as there is only one IISC site located on the undeforming part of the Indian craton. Finally, our attempt to align their GPS velocity field with ITRF shows that velocities of two IGS sites (IISC and LHAS) are in conflict with their ITRF velocities by up to 4–5 mm/yr. It is also surprising to note that some of the regional velocities of Mukul et al. (2010), with longer durations of observations, are more scattered than the data of Jade et al. (2007) from the same sites. In contrast, we find that the data by Jade et al. (2007) at IGS sites (e.g., IISC, LHAS, KIT3, POL2 and SELE) agree well with ITRF velocities up to <1–3 mm/yr. Note that we also did not include the GPS data from Mullick et al. (2009) from the Sikkim Himalayan topographic front. This is because we are uncertain if their detected north–south extension at a rate of 10 mm/yr across a NW-striking fault (presumably a thrust as it parallels to the Himalayan front) is an artifact of landsliding rather than tectonics.

The GPS velocity field of Gan et al. (2007) was derived from a velocity solution of the Crustal Motion Observation Network Project (CMONOC) (Niu et al., 2005) and the published solutions of Paul et al. (2001), Wang et al. (2001) and Banerjee and Bürgmann (2002). Integration of the above solutions was accomplished by tying station velocities at fiducial and collocated sites using a 7-parameter Helmert transformation. Our final GPS solutions are referenced to ITRF2005 (Gan et al., 2007). The largest postfit residuals for the common stations between different datasets are $\sim$2.6 mm/yr and $\sim$1.7 mm/yr for the east and north velocity components. To further improve our GPS solutions we aligned the solutions of Wang et al. (2001) and Banerjee and Bürgmann (2002) with that of Gan et al. (2007) by rigid body rotation under velocity constraints at commonly used fiducial sites (i.e., IISC in India, LHAS in Tibet of western China, and KIT3, POL2 SELE, WUHN, and SHAO in central and eastern Eurasia). The postfit residuals for the horizontal components at these sites are <3 mm/yr. Lastly, we rotate the combined velocity datasets into an India-fixed reference frame while minimizing postfit residuals at sites located in the stable part of the India plate (i.e., IGS, IISC and 7 regional stations in northwest India and southernmost Nepal). This operation results in postfit residuals of <2 mm/yr for the east and north velocity components after excluding 2 sites with larger postfit residuals in the initial solution. Our final velocity solution shows the relative motion of GPS stations with respect to the undeforming northwestern India (Fig. 8). This allows us to compare the GPS velocity field to the Holocene deformation rates across the Himalaya and southern Tibet.

As the Himalayan orogen is an arc in map view, we use a small circle to best represent the trace of the MFT. This was followed by dividing the Himalayan arc into five segments radiating from the pole that generated the MFT arc (Fig. 8). Although the final plots clearly show scatter (Fig. 8), some first-order trends are evident. A right-slip shear rate of 5–10 mm/yr is evident across the western Himalaya, which is broadly compatible with the Holocene and long-term average slip rate over the span of the Karakorum fault ranging from 1 to 10 mm/yr (Searle, 1996; Murphy et al., 2000, 2002; Brown et al., 2002; Phillips et al., 2004; Lacassin et al., 2004; Chevalier et al., 2005; Valli et al., 2007). They are also consistent with the decadal slip rate inferred from a local GPS network survey and an InSar study across the fault (Wright et al., 2004; Valli et al., 2007). A left-slip shear of 2–6 mm/yr parallel to the Himalayan arc occurs across the eastern Himalaya, which is probably accommodated by the newly discovered left-slip Dinggye-Chigu fault zone with a slip rate of 4–8 mm/yr (Li and Yin, 2008). Occurrence of left-slip faulting in the eastern Himalaya is inconsistent with active eastward extrusion of the Tibetan plateau, as it requires a through-going right-slip shear across the whole Himalayan arc (e.g., Armijo et al., 1986). Van der Woerd et al. (2009) reinterpreted the left-lateral drainage deflection pattern along active faults observed by Li and Yin (2008) and suggested that they are related to left-slip faulting. Their reinterpretation was disputed by Li and Yin (2009) and our regional GPS velocity field in Fig. 8 reinforces Li and Yin's (2008) proposal that the Himalayan arc is currently deforming by combined arc-perpendicular shortening and symmetric arc-parallel right-slip shear in the west and left-slip shear in the east across the orogen.

The GPS velocity field also shows a systematic east–west change in the arc-perpendicular shortening rate across the Himalaya and southernmost Tibet, at $\sim$14 mm/yr in the west, $\sim$20 mm/yr in the center, and $\sim$29 mm/yr in the east (Fig. 8). The 14 mm/yr GPS shortening rate across the western swaths is slightly higher than the Holocene shortening rate of 9 ± 3 mm/yr across the western Himalaya (Wesnousky et al., 1999; Malik and Nakata, 2003; Kumar et al., 2006), implying additional active structures such as the Karakorum fault north of the MFT to have accommodated the extra arc-perpendicular shortening. It has been noted that the GPS shortening rate across the central Himalaya is similar to the Holocene slip rate of the MFT across the same longitude, which implies that most of the active convergence of the Himalayan orogen is accommodated by slip on the MFT (Lavé and Avouac, 2000). Our GPS result is consistent with this inference. For the eastern swaths the 29 mm/yr shortening rate relative to fixed India is accommodated by active deformation across the eastern Lhasa block, the Himalayan orogen, and the Shillong plateau. As the eastern Lhasa block is dominated by east–west extension (Zhang et al., 2004) in the GPS velocity field, its active deformation probably contributes little to the total 29-mm/yr shortening. Thus, this shortening must be partitioned in the eastern Himalaya and the Shillong plateau. GPS surveys and modeling of leveling data indicate a present shortening rate of 2–5 mm/yr across the Shillong plateau (Bilham and England, 2001; Paul et al., 2001; Jade et al., 2007). This requires a 24–27 mm/yr shortening rate across the eastern Himalaya, which is consistent with our estimated rate of 23.4 ± 6.2 mm/yr.

It is possible that southern Tibet may be under significant active contraction, which cannot be differentiated completely between the Himalayan shortening caused by the locking of the MFT at depth.

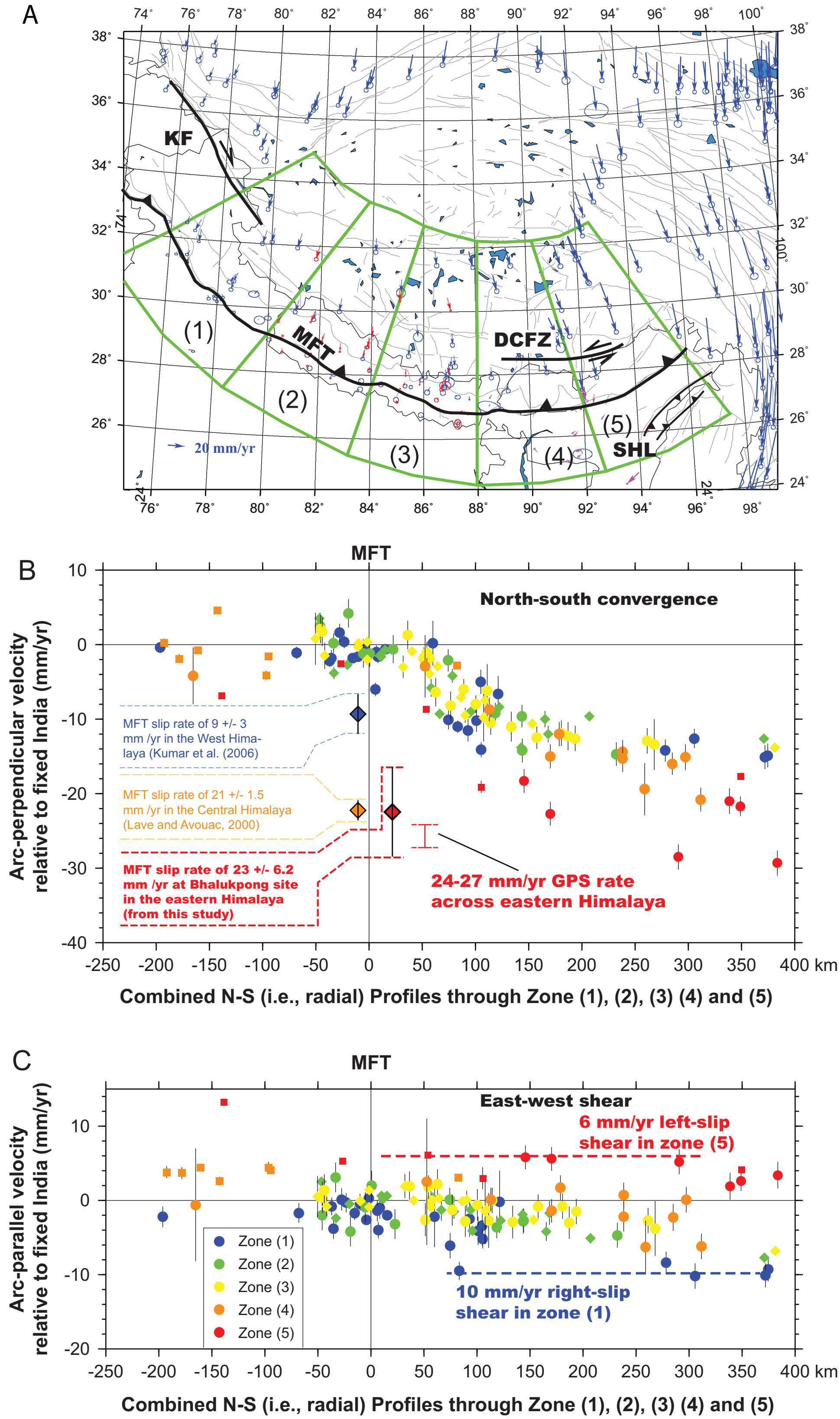

Fig. 8. (A) Map view of GPS velocity field across the Himalayan orogen and southernmost Tibet. The velocity vectors are relative to fixed India. See text for details. Note that the MFT lies at the origin of the horizontal axis. Abbreviations in the figure: KF, Karakorum fault; MFT, Main Frontal Thrust, SHL, the Shillong plateau; DCFZ, Dignnye–Chigu fault zone. (B) Arc-perpendicular velocity distribution relative to fixed India along the swaths of zone (1) to zone (5). Note that the MFT lies at the origin of the horizontal axis. (C) Arc-parallel velocity distribution relative to fixed India along the swaths of zone (1) to zone (5). In both (B) and (C), the color codes from the western to eastern swaths are as following: blue for zone (1), green for zone (2), yellow for zone (3), orange for zone (4), and red for zone (5). (For interpretation of the references to color in this figure legend, the reader is referred to the web version of this article.)

However, recent work by Ader et al. (2012) shows that an elastic back-slip model can satisfactorily explain the observed GPS data across the Himalaya and southern Tibet, with a typical fault locking length of ~100 km. In light of lack of any known contractional structures in southern Tibet north of the Himalaya east of the Karakorum fault (e.g., Taylor and Yin, 2009), we believe that the observed north–south GPS shortening strain across at least the central and eastern Himalaya was dominantly and possibly entirely induced by the locking of the Himalayan Main Frontal Thrust.

Our results have important implications for the development of the Tibetan plateau. Although the plateau currently displays a strong east–west asymmetry in its north–south width, this geometry *could not* have been induced by an eastward increase in the India–Asia convergence rate if our observation of the MFT-slip-rate distribution along the Himalayan arc can be generalized to the geologic past. This is because the asymmetric effect of the plate boundary convergence rate, about 10 mm/yr difference at the eastern and western ends of the Himalaya (Molnar and Stock, 2009), has been "filtered" out by along-strike variation of deformation within the Himalaya. Thus, alternative explanations such as a change in polarity of thrust systems along the northern margin of the Tibetan plateau (Cowgill et al., 2003) and partitioning of inhomogeneous shortening across central Asia should be considered (e.g., Neil and Houseman, 1997). When evaluating seismic hazards, Himalayan earthquake geologists have implicitly assumed that the MFT has a uniform slip rate everywhere across the Himalayan topographic front (e.g., Kumar et al., 2010). However, if the shortening rate of the MFT zone increases eastward and the repeated major earthquakes have similar magnitudes, the MFT along the central and eastern Himalayan front would have shorter recurrence intervals and host more frequent large earthquakes than those along the MFT in the western Himalaya.

7. Conclusions

Restoration of a balanced cross section and the observed growth–strata relationship require a minimum shortening rate of 13 mm/yr across the eastern Himalayan orogenic belt since ~2 Ma. Topographic surveying and dating of Holocene river terraces in the Bhalukpong area of the eastern Himalaya constrain a minimum total shortening rate across the 10 km wide Main Frontal Thrust (MFT) zone to be at 23.4 ± 6.2 mm/yr. This total shortening rate is similar to the GPS shortening rate across southeastern Tibet and the eastern Himalaya, indicating that the MFT zone is the dominant structure accommodating nearly all active deformation of the region. The total shortening rate across the 10 km wide MFT zone in the eastern Himalaya is distributed across three active structures: at ~8.4 mm/yr on the Bhalukpong thrust in the north, at ~10 mm/yr across the Balipara growing anticline in the center, and at ~5 mm/yr on the Nameri thrust in the south. Although the obtained shortening rate of 23.4 ± 6.2 mm/yr across the eastern Himalaya is similar to or greater than the estimated slip rate of 21 ± 1.5 mm/yr for the MFT zone in the central Himalaya, this rate is significantly higher than the slip rate of 9 ± 3 mm/yr for the MFT zone in the western Himalaya. This observation supports an interpretation that the active growth of the Himalayan orogen is driven by an eastward increase in the plate convergence rate between India and Asia. It also supports the proposal of Lavé and Avouac (2000) that active Himalayan shortening is mostly accommodated by slip along the discrete MFT zone bounding the Himalayan front

Acknowledgments

This work was supported by a Grant from the Tectonics Program of the US National Science Foundation awarded to An Yin and an Indian CAS-UGC Grant awarded to the Department of Geology, University of Delhi. The original draft of the manuscript was greatly improved by the constructive comments of an anonymous reviewer, Roger Bilham, and Peter DeCelles.

References

Acharyya, S.K., 1998. Thrust tectonics and evolution of domes and the syntaxis in eastern Himalaya, India. J. Nepal Geol. Soc. 18, 1–17.
Acharyya, S.K., Ghosh, S.C., Ghosh, R.N., 1975. Stratigraphy of Assam-Valley India—discussion. AAPG Bull. 59, 2046–2050.
Acharyya, S.K., Sengupta, S., 1998. The structure of the Siang window, its evolution and bearing on the nature of eastern syntaxis of the Himalaya. Natl. Acad. Sci. Lett. India 21, 177–192.
Ader, T., Avouac, J.P., Liu-Zeng, J., Lyon-Caen, H., Bollinger, L., Galetzka, J., Genrich, J., Thomas, M., Chanard, K., Sapkota, S.N., Rajaure, S., Shrestha, P., Ding, L., Flouzat, M., 2012. Convergence rate across the Nepal Himalaya and interseismic coupling on the Main Himalayan Thrust: implications for seismic hazard. J. Geophys. Res. 117, B04403, http://dx.doi.org/10.1029/2011JB009071.
Amos, C.B., Burbank, D.W., 2007. Channel width response to differential uplift. J. Geophys. Res. 112, F02010, http://dx.doi.org/10.1029/2006JF000672.
Angelier, J., Baruah, S., 2009. Seismotectonics in Northeast India: a stress analysis of focal mechanism solutions of earthquakes and its kinematic implications. Geophys. J. Int. 178, 303–326.
Armijo, R., Tapponnier, P., Mercier, J.L., Han, T.-L., 1986. Quaternary extension in southern Tibet: field observations and tectonic implications. J. Geophys. Res. 91, 13803–13872.
Avouac, J.P., 2003. Mountain building, erosion, and the seismic cycle in the Nepal Himalaya. Adv. Geophys. 46, 1–80.
Baker, D.M., Lillie, R.J., Yeats, R.S., Johnson, G.D., Yousuf, M., Zamin, A.S.H., 1988. Development of the Himalayan frontal thrust zone: Salt Range, Pakistan. Geology 16, 3–7.
Banerjee, P., Bürgmann, R., 2002. Convergence across the northwest Himalaya from GPS measurements. Geophys. Res. Lett. 29 (16), 52, http://dx.doi.org/10.1029/2002GL015184.
Bhargava, O.N., 1995. The Bhutan Himalaya: A Geological Account, vol. 39. Geological Survey of India, Bangalore, Special Publication 244 pp.
Bilham, R., 1995. Location and magnitude of the 1833 Nepal earthquake and its relation to the rupture zones of contiguous great Himalayan earthquakes. Curr. Sci. 69, 155–187.
Bilham, R., 2004. Earthquakes in India and the Himalaya: tectonics, geodesy and history. Ann. Geophys. 47, 839–858.
Bilham, R., Ambraseys, N., 2005. Apparent Himalayan slip deficit from the summation of seismic moments for Himalayan earthquakes, 1500–2000. Curr. Sci. 88, 1658–1663.
Bilham, R., England, P., 2001. Plateau "pop-up" in the great 1897 Assam earthquake. Nature 410, 806–809.
Bilham, R., Larson, K., Freymueller, J., 1997. GPS measurements of present day convergence across the Nepal Himalaya. Nature 386, 61–64, http://dx.doi.org/10.1038/386061a0.
Bilham, R., Blume, F., Bendick, R., Gaur, V.K., 1998. Geodetic constraints on the translation and deformation of India: implications for future great Himalayan earthquakes. Curr. Sci. 74, 213–229.
Bilham, R., Larson, K., Lai, X., You, X., Niu, Z., Wu, J., Li, Y., Liu, J., Yang, Z., Chen, Q., 2001. Science. Present day crustal deformation in China constrained by Global Positioning System (GPS) measurements 294, 574–577.
Biswas, S., Isabelle, C., Grujic, D., Hager, C., Stockli, D., Grasemann, B., 2007. Exhumation and uplift of the Shillong Plateau and its influence on the eastern Himalayas: new constraints from apatite and zircon (U–Th–[Sm])/He and apatite fission track analyses. Tectonics 26, TC6013, http://dx.doi.org/10.1029/2007TC002125.
Brown, C.J., 1912. A geologic reconnaissance through the Dihang Valley, being the geological result of the Abor Expedition, 1911–12. Rec. Geol. Surv. India 42, 231–264.
Brown, E.T., Bendick, R., Bourles, D.L.,Gaur,V., Molnar, P., Raisbeck, G.M., Yiou, F., 2002. Slip rates of the Karakorum Fault, Ladakh, India, determined using cosmic ray exposure dating of debris flows and moraines. J. Geophys. Res. 107, pp.7-1 to 7-13, http://dx.doi.org/10.1029/2000JB000100.
Bull, W., 1991. Geomorphic Response to Climatic Change. Oxford University Press, New York, 326 pp.
Burbank, D.W., Beck, R.A., Mulder, T., 1996. The Himalayan foreland basin. In: Yin, A., Harrison, T.M. (Eds.), The Tectonics of Asia. Cambridge University Press, New York, pp. 149–188.
Carosi, R., Montomoli, C., Visona, D., 2007. A structural transect in the Lower Dolpo: insights on the tectonic evolution of western Nepal. J. Asian Earth Sci. 29, 407–423.
Chambers, J., Parrish, R., Argles, T., Harris, N., Horstwood, M., 2011. A short-duration pulse of ductile normal shear on the outer South Tibetan detachment in Bhutan: alternating channel flow and critical taper mechanics of the eastern Himalaya. Tectonics 30, TC2005, http://dx.doi.org/10.1029/2010TC002784.
Chen, W.-P., Molnar, P., 1977. Seismic moments of major earthquakes and the average rate of slip in central Asia. J. Geophys. Res. 82, 2945–2969.

Chevalier, M.L., Ryerson, F.J., Tapponnier, P., Finkel, R.C., Van der Woerd, J., Li, H.B., Liu, Q., 2005. Slip-rate measurements on the Karakorum Fault may imply secular variations in fault motion. Science 307, 411–414.

Chirouze, F., Dupont-Nivet, G., Huyghe, P., van der Beek, P., Chakraborti, T., Bernet, M., Erens, V., 2012. Magnetostratigraphy of the Neogene Siwalik Group in the far eastern Himalaya: Kameng section, Arunachal Pradesh, India. J. Asia Earth Sci. 44, 117–135, http://dx.doi.org/10.1016/j.jseaes.2011.05.016.

Clark, M.K., Bilham, R., 2008. Miocene rise of the Shillong Plateau and the beginning of the end for the eastern Himalaya. Earth Planet. Sci. Lett. 269, 337–350, http://dx.doi.org/10.1016/j.epsl.2008.01.045.

Cook, K.L., Whipple, K.X., Heimsath, A.M., Hanks, T.C., 2009. Rapid incision of the Colorado River in Glen Canyon—insights from channel profiles, local incision rates, and modeling of lithologic controls. Earth Surf. Processes Landforms 34, 994–1010.

Copley, A., Avouac, J.-P., Royer, J.-Y., 2010. India–Asia collision and the Cenozoic slowdown of the Indian plate: implications for the forces driving plate motions. J. Geophys. Res. 115, B03410, http://dx.doi.org/10.1029/2009JB006634.

Cowgill, E., Yin, A., Harrison, T.M., Wang, X.F., 2003. Reconstruction of the Altyn Tagh fault based on U–Pb geochronology: role of back thrusts, mantle sutures, and heterogeneous crustal strength in forming the Tibetan Plateau. J. Geophys. Res. 108, B072346, http://dx.doi.org/10.1029/2002JB002080.

Daniel, C.G., Hollister, L.S., Parrish, R.R., Grujic, D., 2003. Exhumation of the Main Central Thrust from lower crustal depths, Eastern Bhutan Himalaya. J. Metamorphic Geol. 21, 317–334.

Das Gupta, A.B., Biswas, A.K., 2000. Geology of Assam, Geological Society of India 169 pp.

Davidson, C., Grujic, D.E., Hollister, L.S., Schmid, S.M., 1997. Metamorphic reactions related to decompression and synkinematic intrusion of leucogranite, High Himalayan Crystallines, Bhutan. J. Metamorphic Geol. 15, 593–612.

Devi, R.K.M., Bhakuni, S.S., Bora, P.K., 2011. Tectonic implication of drainage set-up in the Sub-Himalaya: a case study of Papumpare district, Arunachal Himalaya, India. Geomorphology 127, 14–31.

Drukpa, D., Velasco, A.A., Doser, D.I., 2006. Seismicity in the Kingdom of Bhutan (1937–2003): evidence for crustal transcurrent deformation. J. Geophys. Res. 111, B06301, http://dx.doi.org/10.1029/2004JB003087.

Duvall, A., Kirby, E., Burbank, D.W., 2004. Tectonic and lithologic controls on bedrock channel profiles and processes in coastal California. J. Geophys. Res. 109, F03002, http://dx.doi.org/10.1029/2003JF000086.

Edwards, M.A., Kidd, W.S.F., Li, J.X., Yu, Y.J., Clark, M., 1996. Multi-stage development of the southern Tibet detachment system near Khula Kangri. New data from Gonto La. Tectonophysics 260, 1–19, http://dx.doi.org/10.1016/0040-1951(96)00073-X.

Evans, P., 1964. The tectonic framework of Assam. Geol. Soc. India Bull. 5, 80–96.

Feldl, N., Bilham, R., 2006. Great Himalayan earthquakes and the Tibetan plateau. Nature 444, 165–170.

Gan, W.J., Zhang, P.Z., Shen, Z.K., Niu, Z.J., Wang, M., Wan, Y.G., Zhou, D.M., Cheng, J., 2007. Present-day crustal motion within the Tibetan Plateau inferred from GPS measurements. J. Geophys. Res. 112 (B8), B08416, http://dx.doi.org/10.1029/2005JB004120.

Gansser, A., 1964. The Geology of the Himalayas. Wiley Interscience, New York 289 pp.

Gansser, A., 1983. Geology of the Bhutan Himalaya. Birkhaüser Verlag, Boston 180 pp.

Goodwin-Austen, H.H., 1864. Geological notes on part of the North-Western Himalayas. Q. J. Geol. Soc. London 20, 383–387.

Grujic, D., Casey, M., Davidson, C., Hollister, L.S., Kundig, R., Pavlis, T., Schmid, S., 1996. Ductile extrusion of the Higher Himalayan Crystalline in Bhutan: evidence from quartz microfabrics. Tectonophysics 260, 21–43.

Grujic, D., Hollister, L.S., Parrish, R.R., 2002. Himalayan metamorphic sequence as an orogenic channel: insight from Bhutan. Earth Planet. Sci. Lett. 198, 177–191.

Grujic, D., Coutand, I., Bookhagen, B., Bonnet, S., Blythe, A., Duncan, C., 2006. Climatic forcing of erosion, landscape, and tectonics in the Bhutan Himalayas. Geology 34, 801–804.

Gupta, R.P., Sen, A.K., 1988. Imprints of Ninety-East Ridge in the Shillong Plateau, Indian Shield. Tectonophysics 154 (335–341), 90111–90114, http://dx.doi.org/10.1016/0040-1951(88).

Hollister, L.S., Grujic, D., 2006. Pulsed channel flow in Bhutan. In: Law, R.D., Searle, M.P., Godin, L. (Eds.), Channel Flow, Extrusion, and Exhumation in Continental Collision Zones, vol. 268. Geological Society of London Special Publications, London, pp. 415–423.

Hussain, A., Yeats, R.S., MonaLisa, 2009. Geological setting of the 8 October 2005 Kashmir earthquake. J. Seismol. 13, 315–325.

Jade, S., Mukul, M., Bhattacharyya, A.K., Vijayan, S.J., Kumar, A., Tiwari, R.P., Kumar, A., Kalita, S., Sahu, S.C., Krishna, A.P., Gupta, S.S., Murthty, M.V.R.L., Gaur, V.K., 2007. Estimates of interseismic deformation in Northeast India from GPS measurements. Earth Planet. Sci. Lett. 263, 221–234.

Jain, A.K., Thakur, V.C., Tandon, S.K., 1974. Stratigraphy and structure of the Siang district, Arunachal (NEFA) Himalaya. Himalayan Geol. 4, 28–60.

Jangpangi, B.S., 1974. Stratigraphy and tectonics of parts of eastern Bhutan. Himalayan Geol. 4, 117–136.

Jaswal, T., Lillie, R., Lawrence, R., 1997. Structure of the northern Potwar deformed zone. Pak.: Am. Assoc. Pet. Geol. Bull. 81, 308–328.

Jouanne, F., Mugnier, J.L., Gamond, J.F., LeFort, P., Pandey, M.R., Bollinger, L., Flouzat, M., Avouac, J.P., 2004. Current shortening across the Himalayas of Nepal. Geophys. J. Int. 157, 1–14.

Kaneda, H., Nakata, T., Tsutsumi, H., Kondo, H., Sugito, N., Awata, Y., Akhtar, S.S., Majid, A., Khattak, W., Awan, A.A., Yeats, R.S., Hussain, A., Ashraf, M., Wesnousky, S.G., Kausar, A.B., 2008. Surface rupture of the 2005 Kashmir, Pakistan, earthquake, and its active tectonic implications. Bull. Seism. Soc. Am. 98, 521–557, http://dx.doi.org/10.1785/0120070073.

Kayal, J.R., De, R., 1991. Microseismicity and tectonics in northeast India. Bull. Seism. Soc. Am 81, 131–138.

Kayal, J.R., Arefiev, S.S., Barua, S., Hazarika, D., Gogoi, N., Kumar, A., Chowdhury, S.N., Kalita, S., 2006. Shillong Plateau earthquake in northeast India region: complex tectonic model. Curr. Sci. 91, 109–114.

Kellett, D.A., Grujic, D., Erdmann, S., 2009. Miocene structural reorganization of the South Tibetan detachment, eastern Himalaya: implications for continental collision. Lithosphere 1, 259–281.

Kellett, D.A., Grujic, D., Warren, C., Cottle, J., Jamieson, R., Tensin, T., 2010. Metamorphic history of a syn-convergent orogen-parallel detachment: the South Tibetan detachment system, Bhutan Himalaya. J. Metamorphic Geol. 28, 785–808.

Kumar, G., 1997. Geology of Arunachal Pradesh. Geological Society of India, Bangalore.

Kumar, D., Mamallan, R., Dwivedy, K.K., 1996. Carbonatite magmatism in northeast India. J. Southeast Asian Earth Sci. 13, 145–158, http://dx.doi.org/10.1016/0743-9547(96)00016-5.

Kumar, S., Wesnousky, S.G., Rockwell, T.K., Briggs, R.W., Thakur, V.C., Jayangondaperumal, R., 2006. Paleoseismic evidence of great surface rupture earthquakes along the Indian Himalaya. J. Geophys. Res. 111, B03304, http://dx.doi.org/10.1029/2004JB003309.

Kumar, S., Wesnousky, S.G., Jayangondaperumal, R., Nakata, T., Kumahara, Y., Singh, V., 2010. Paleoseismological evidence of surface faulting along the northeastern Himalayan front, India: timing, size, and spatial extent of great earthquakes. J. Geophys. Res. 115, B12422, http://dx.doi.org/10.1029/2009JB006789.

Lacassin, R., Valli, F., Arnaud, N., Leloup, P.H., Papuette, J.L., Haibing, L., Tapponnier, P., Chevalier, M.-L., Guillot, S., Mahéo, G., Zhiqin, X., 2004. Large-scale geometry, offset and kinematic evolution of the Karakorum fault, Tibet. Earth Planet. Sci. Lett. 219, 255–269.

La Touche, T.D., 1883. Notes on the geology of the Aka Hills, Assam. Rec. Geol. Surv. India 18, 121–124.

Lavé, J., Avouac, J.P., 2000. Active folding of fluvial terraces across the Siwaliks Hills, Himalayas of central Nepal. J. Geophys. Res. 105, 5735–5770.

Lavé, J., Avouac, J.P., 2001. Fluvial incision and tectonic uplift across the Himalayas of central Nepal. J. Geophys. Res. 106, 26561–26591.

Lavé, J., Yule, d., Sopkota, S., Basant, K., Madden, C., Attal, M., Pandey, R., 2005. Evidence for a great medieval earthquake ($\sim$1100 A.D.) in the central Himalayas, Nepal. Science 307, 1302–1305.

Lay, T., Kanamori, H., Ammon, C.J., Nettles, M., Ward, S.N., Aster, R.C., Beck, S.L., Bilek, S.L., Brudzinski, M.R., Butler, R., DeShon, H.R., Ekstrom, G., Satake, K., Sipkin, S., 2005. The Great Sumatra–Andaman Earthquake of 26 December 2004. Science 308, 1127–1133.

Le Dain, A.Y., Tapponnier, P., Molnar, P., 1984. Active faulting and tectonics of Burma and surrounding regions. J. Geophys. Res. 89, 453–472.

Li, D.W., Yin, A., 2008. Orogen-parallel, active left-slip faults in the Eastern Himalaya: implications for the growth mechanism of the Himalayan arc. Earth Planet. Sci. Lett. 274, 258–267.

Li, D.W., Yin, A., 2009. Reply to "A Comment on "Orogen-Parallel, Active Left-Slip Faults in the Eastern Himalaya: Implications for the Growth Mechanism of the Himalayan Arc" by Li and Yin (Earth Planet. Sci. Lett. 274 (2008) 258–267)" by Van der Woerd et al. Earth Planet. Sci. Lett. 285, 223–223.

Long, S., McQuarrie, N., 2010. Placing limits on channel flow: insights from the Bhutan Himalaya. Earth Planet. Sci. Lett. 290, 375–390.

Long, S., McQuarrie, N., Tobgay, T., Rose, C., Gehrels, G., Grujic, D., 2011a. Tectonostratigraphy of the Lesser Himalaya of Bhutan: implications for the along-strike stratigraphic continuity of the northern Indian margin. Geol. Soc. Am. Bull. 123, 1406–1426, http://dx.doi.org/10.1130/B30202.1.

Long, S., McQuarrie, N., Tobgay, T., Hawthorne, J., 2011b. Quantifying internal strain and deformation temperature in the eastern Himalaya, Bhutan: implications for the evolution of strain in thrust sheets. J. Struct. Geol. 33, 579–608.

MaClaren, J.M., 1904. The Geology of Upper Assam. Rec. Geol. Surv. India XXXI, 179–232.

Malik, J.N., Nakata, T., 2003. Active faults and related late quaternary deformation along the northwestern Himalayan Frontal Zone, India. Ann. Geophys. 46, 917–936.

Meyer, M.C., Wiesmayr, G., Brauner, M., Hausler, H., Wangda, D., 2006. Active tectonics in Eastern Lunana (NW Bhutan): implications for the seismic and glacial hazard potential of the Bhutan Himalaya. Tectonics 25, TC3001, http://dx.doi.org/10.1029/2005TC001858.

McQuarrie, N., Robinson, D., Long, S., Tobgay, T., Grujic, D., Gehrels, G., Ducea, M., 2008. Preliminary stratigraphic and structural architecture of Bhutan: implications for the along strike architecture of the Himalayan system. Earth Planet. Sci. Lett. 272, 105–117.

Mitra, S., Priestley, K., Bhattacharyya, A.K., Gaur, V.K., 2005. Crustal structure and earthquake focal depths beneath northeastern India and southern Tibet. Geophys. J. Int. 160, 227–248, http://dx.doi.org/10.1111/j.1365-246X.2004.02470.x.

Molnar, P., Stock, J.M., 2009. Slowing of India's convergence with Eurasia since 20 Ma and its implications for Tibetan mantle dynamics. Tectonics 28, TC3001, http://dx.doi.org/10.1029/2008TC00227.

Mukul, M, Jade, S., Bhattacharya, A.K., Bhusan, K., 2010. Crustal Shortening in Convergent Orogens: insights from Global Positioning System (GPS) measurements in Northeast India. J. Geol. Soc. India 75, 302–312.

Mullick, M., Riguzzi, F., Mukhopadhyay, D., 2009. Estimates of motion and strain rates across active faults in the frontal part of eastern Himalayas in North Bengal from GPS measurements. Terra Nova 21, 410–415.
Murphy, M.A., Yin, A., Kapp, P., Harrison, T.M., Lin, D., Guo, J.H., 2000. Southward propagation of the Karakoram fault system, southwest Tibet: timing and magnitude of slip. Geology 28, 451–454.
Murphy, M.A., Yin, A., Kapp, P., Harrison, T.M., Manning, C.E., Ryerson, F.J., Ding, L., Guo, J.H., 2002. Structural evolution of the Gurla Mandhata detachment system, southwest Tibet: implications for the eastward extent of the Karakoram fault system. Geol. Soc. Am. Bull. 114, 428–447.
Nakata, T., 1989. Active faults of the Himalaya of India and Nepal. In: Malinconico, L.L., Lillie, R.J. (Eds.), Tectonics of the Western Himalayas, vol. 232. Geol. Soc. Am. Bull. Spec. Pap.
Nandy, D.R., 2001. Geodynamics of Northeastern India and the Adjoining Region. ACB publications, Lake Town, Calcutta.
Neil, E.A., Houseman, G.A., 1997. Geodynamics of the Tarim Basin and the Tian Shan in central Asia. Tectonics 16, 571–584.
Niu, Z, Wang, M., Sun, H.R., Sun, J.Z., You, X.Z., Gan, W.J., Xue, G.J., Hao, J.X., Xin, S.H., Wang, Y.Q., Wang, Y., Li, B., 2005. Contemporary velocity field of crustal movement of Chinese mainland from Global Positioning System measurements. Chin. Sci. Bull. 50 (9), 939–941.
Paul, J., Burgman, R., Gaur, V.K., Bilham, R., Larson, K.M., Ananda, M.B., Jade, S., Mukal, M., Anupama, T.S., Satyal, G., Kumar, D., 2001. The motion and active deformation of India. Geophys. Res. Lett. 28, 647–650.
Ojha, T.P., Butler, R.F., Quade, J., DeCelles, P.G., Richards, D., Upreti, B.N., 2000. Magnetic polarity stratigraphy of the Neogene Siwalik Group at Khutia Khola, far-western Nepal. Bull. Geol. Soc. Am. 112, 424–434.
Ojha, T.P., Butler, R.F., DeCelles, P.G., Quade, J., 2009. Magnetic polarity stratigraphy of the Neogene foreland basin deposits of Nepal. Basin Res. 21, 61–90.
Phillips, R.J., Parrish, R.R., Searle, M.P., 2004. Age constraints on ductile deformation and long-term slip rates along the Karakoram fault zone, Ladakh. Earth Planet. Sci. Lett. 226, 305–319.
Ponraj, M., Miura, S., Reddy, C.D., Amirtharaj, S., Mahajan, S.H., 2011. Slip distribution beneath the Central and Western Himalaya inferred from GPS observations. Geophys. J. Int. 185, 724–736, http://dx.doi.org/10.1111/j.1365-246X.2011.04958.x.
Powers, P.M., Lillie, R.J., Yeats, R.S., 1998. Structure and shortening of the Kangra and Dehra Dun reentrants, Sub-Himalaya, India. Geol. Soc. Am. Bull. 110, 1010–1027.
Rajendran, C.P., Rajendran, K., Duarah, B.P., Baruah, S., Earnest, A., 2004. Interpreting the style of faulting and paleoseismicity associated with the 1897 Shillong, northeast India, earthquake: implications for regional tectonics. Tectonics 23, 1–12, http://dx.doi.org/10.1029/2003TC001605.
Ray, S.K., Bandyopadhyay, B.K., Razdan, R.K., 1989. Tectonics of the Shumar allochton in eastern Bhutan. Tectonophysics 169, 51–58.
Ray, S.K., 1995. Scaling properties of thrust fault traces in the Himalayas and inferences on thrust fault growth. J. Struct. Geol. 28, 1307–1315.
Rhodes, E.J., 2011. Optically stimulated luminescence dating of sediments over the past 200,000 years. Annu. Earth Planet. Sci. Rev. 39, 461–488.
Richards, A., Parrish, R., Harris, N., Argles, T., Zhang, L., 2006. Correlation of lithotectonic units across the eastern Himalaya, Bhutan. Geology 34, 341–344.
Roberts, G.G., White, N., 2010. Estimating uplift rate histories from river profiles using African examples. J. Geophys. Res. 115, B02406, http://dx.doi.org/10.1029/2009JB006692.
Searle, M.P., 1996. Geological evidence against large-scale pre-Holocene offsets along the Karakoram Fault: implications for the limited extrusion of the Tibetan plateau. Tectonics 15, 171–186.
Seeber, L., Armbruster, J., 1981. Great detachment earthquakes along the Himalayan Arc and longterm forecasting, in earthquake prediction: an international review. In: Simpson, D.W., Richards, P.G. (Eds.), Maurice Ewing Series, vol. 4. AGU, Washington, D.C., pp. 259–277.
Srivastava, P., Misra, D.K., 2008. Morpho-sedimentary records of active tectonics at the Kameng river exit, NE Himalaya. Geomorphology 96, 187–198.
Srivastava, P., Bhakuni, S.S., Luirei, K, Misra, D.K., 2009. Morpho-sedimentary records at the Brahmaputra River exit, NE Himalaya: climate–tectonic interplay during the Late Pleistocene–Holocene. J. Q. Sci 24, 175–188.
Srivastava, R.K., Sinha, A.K., 2004a. Geochemistry of Early Cretaceous alkaline ultramafic-mafic complex from Jasra, Karbi Anglong, and Shillong Plateau northeastern India. Gondwana Res. 7, 549–561, http://dx.doi.org/10.1016/S1342-937X(05)70805-4.
Srivastava, R.K., Sinha, A.K., 2004b. Early Cretaceous Sung Valley ultramafic–alkaline–carbonatite complex, Shillong Plateau, northeastern India: petrological and genetic significance. Miner. Pet. 80, 241–263, http://dx.doi.org/10.1007/s00710-003-0025-1.
Srivastava, R.K., Heaman, L.A., Sinha, A.K., Sun, S.H., 2005. Emplacement age and isotope geochemistry of Sung Valley alkaline–carbonatite complex, Shillong Plateau, northeastern India: implications for primary carbonate melt and genesis of the associated silicate rocks. Lithos 81, 33–54, http://dx.doi.org/10.1016/j.lithos.2004.09.017.
Stüwe, K., Foster, D., 2001. Ar-40/Ar-39, pressure, temperature and fission-track constraints on the age and nature of metamorphism around the Main Central Thrust in the eastern Bhutan Himalaya. J. Asian Earth Sci. 19, 85–95.
Suppe, J., 1983. Geometry and kinematics of fault-bend folding. Am. J. Sci. 283, 684–721.
Swapp, S.M., Hollister, L.S., 1991. Inverted metamorphism within the Tibetan slab of Bhutan—evidence for a tectonically transported heat source. Can. Mineral. 29, 1019–1041.
Szeliga, W., Hough, S., Martin, S., Bilham, R., 2010. Intensity, magnitude, location, and attenuation in India for felt earthquakes since 1762. Bull. Seismol. Soc. Am. 100, 570–584, http://dx.doi.org/10.1785/0120080329.
Tandon, A.N., 1955. The direction of faulting in the great Assam earthquake of 15 August 1950. Indian J. Meteorol. Geophys. 6, 61–64.
Tangri, S.K., Bhargava, O.N., Pande, A.C., 2003. Late Precambrian Early Cambrian trace fossils from Tethyan Himalaya, Bhutan and their bearing on the Precambrian–Cambrian boundary. J. Geol. Soc. India 62, 708–716.
Taylor, M.H., and Yin, A., 2009, Active faulting on the Tibetan Plateau and sounding regions: Relationships to earthquakes, contemporary strain, and late Cenozoic volcanism. Geosphere, v. 5; no. 3; p. 199 -214; http://dx.doi.org/10.1130/GES00217.1.
Thakur, V.C., 1986. Tectonic zonation and regional framework of eastern Himalaya. Sci. de la Terre 47, 347–360.
Thakur, V.C., Jain, A.K., 1974. Tectonics of eastern region. Curr. Sci. India 43, 783–785.
Tripathi, C., Dungrakoti, B.D., Jain, L.S., Kaura, S.C., Basu Roy, S., Laxmipathi, N.S., 1982. Geology of Dirang–Doimara area, Kemeng district, Arunachal Pradesh with special reference to structure and tectonics. Himalayan Geol. 10, 353–365.
Turowski, J., Lague, M.D., Crave, A., Hovius, N., 2006. Experimental channel response to tectonic uplift. J. Geophys. Res. 111, F03008, http://dx.doi.org/10.1029/2005JF000306.
Turowski, J.M., Lague, D., Hovius, N., 2009. Response of bedrock channel width to tectonic forcing: insights from a numerical model, theoretical considerations, and comparison with field data. J. Geophys. Res. 114, F03016, http://dx.doi.org/10.1029/2008JF001133.
Valli, F., Arnaud, N., Leloup, P.H., Sobel, E.R., Mahéo, G., Lacassin, R., Guillot, S., Li, H., Tapponnier, P., Xu, Z., 2007. Twenty million years of continuous deformation along the Karakorum fault, western Tibet: a thermochronological analysis. Tectonics 26, 1–26, http://dx.doi.org/10.1029/2005TC001913.
Van der Woerd, J., Leloup, Ph.-H., Liu-Zeng, J., Lacassin, R., Tapponnier, P., 2009. A Comment on "Orogen-Parallel, Active Left-Slip Faults in the Eastern Himalaya: Implications for the Growth Mechanism of the Himalayan Arc" by Li and Yin (Earth Planet. Sci. Lett. 274 (2008) 258–267). Earth Planet. Sci. Lett. 285 (2009) 217–222.
Verma, P.K., Tandon, S.K., 1976. Geological observations in parts of Kameng district, Arunachal Pradesh (NEFA). Himalayan Geol. 6, 259–286.
Wang, Q., Zhang, P.Z., Freymueller, J.T., Bilham, R, Larson, K.M., Lai, X., You, X., Niu, Z., Wu, J., Li, Y., Liu, J., Yang, Z., Chen, Q., 2001. Present-day crustal deformation in China constrained by global positioning system measurements. Science 294, 574–577.
Wesnousky, S.G., Kumar, S., Mohindra, R., Thakur, V.C., 1999. Uplift and convergence along the Himalayan Frontal Thrust of India. Tectonics 18, 967–976.
White, N.M., Pringle, M., Garzanti, E., Bickle, M., Najman, Y., Chapman, H., Friend, P., 2002. Constraints on the exhumation and erosion of the High Himalayan Slab, NW India, from foreland basin deposits. Earth Planet. Sci. Lett. 195, 29–44.
Wright, T.J., Parsons, B., England, P.C., Fielding, E.J., 2004. InSAR observations of low slip rates on the major faults of western Tibet. Science 305 (5681), 236–239.
Yeats, R.S., Thakur, V.C., 2008. Active faulting south of the Himalayan front: establishing a new plate boundary. Tectonophysics 453, 63–73.
Yeats, R.S., Nakata, T., Farah, A., Fort, M., Mirza, M.A., Pandey, M.R., Stein, R.S., 1992. The Himalayan frontal fault system. In: Bucknam, R.C., Hancock, P.L. (Eds.), Major Active Faults of the World: Results of IGCP Project 206. Annales Tectonicae, pp. 85–98 (supp. to v. VI).
Yin, A., 2006. Cenozoic tectonic evolution of the Himalayan orogen as constrained by along-strike variation of structural geometry, exhumation history, and foreland sedimentation. Earth Sci. Rev. 76, 1–131.
Yin, A., 2010. Cenozoic tectonic evolution of Asia: a preliminary synthesis. Tectonophysics 488, 293–325.
Yin, A., Taylor, M.H., 2011. Mechanics of V-shaped conjugate strike-slip faults and the corresponding continuum mode of continental deformation. Geol. Soc. Am. Bull. 123, 1798–1821, http://dx.doi.org/10.1130/B30159.1.
Yin, A., Dubey, C.S., Webb, A.A.G., Kelty, T.K., Grove, M., Gehrels, G.E., Burgess, W.P., 2010a. Geologic correlation of the Himalayan orogen and Indian craton (part 1): structural geology, U–Pb Zircon geochronology, and tectonic evolution of the Shillong Plateau and its neighboring regions in NE India. Geol. Soc. Am. Bull. 122, 336–359, http://dx.doi.org/10.1130/B26460.1.
Yin, A., Dubey, C.S., Kelty, T.K., Webb, A.A.G., Harrison, T.M., Chou, C.Y., Célérier, J., 2010b. Geologic correlation of the Himalayan orogen and Indian craton (part 2): structural geology, geochronology and tectonic evolution of the eastern Himalaya. Geol. Soc. Am. Bull. 122, 360–395, http://dx.doi.org/10.1130/B26461.1.
Zhang, P., Shen, Z., Wang, M., Gan, W., Bürgmann, R., Molnar, P., 2004. Continuous deformation of the Tibetan Plateau from global positioning system data. Geology 32, 809–812.